Imaging nanoparticles on graphene with eV-TEM

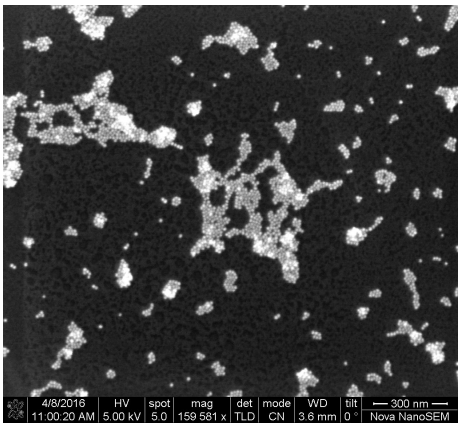

THESIS

submitted in partial fulfillment of the
requirements for the degree of

BACHELOR OF SCIENCE
in
PHYSICS

Author :	C.S. Remeijer
Student ID :	0778745
Supervisor :	Dr. ir. S.J. van der Molen
	D. Geelen MSc
2^{nd} corrector :	Dr. ir. S.J.T. van Noort

Leiden, The Netherlands, 18-08-2016

Imaging nanoparticles on graphene with eV-TEM

C.S. Remeijer

Huygens-Kamerlingh Onnes Laboratory, Leiden University
P.O. Box 9500, 2300 RA Leiden, The Netherlands

18-08-2016

Abstract

We determined the spatial resolution of the new very low energy transmission electron microscopy technique called eV-TEM [1] and used it to image gold nanoparticles deposited on graphene in order to determine whether it is possible to image for example DNA and proteins with low energy electrons.

By transferring graphene to a flat grid with small circular holes in it we created new samples with flatter, less wrinkled graphene that make performing eV-TEM measurements on graphene easier and increase their quality. We improved the alignment of the imaging system of the microscope and determined the resolution of eV-TEM using the new samples to image graphene. We found a method to deposit 10 nm gold nanoparticles on graphene suitable for eV-TEM measurements and a method to deposit ferritin on graphene that we should be able to image as well.

We conclude that the spatial resolution of the current set-up of eV-TEM is 10 nm and that it is possible to image gold nanoparticles deposited on graphene with eV-TEM.

Contents

Chapter 1

Introduction

Electron microscopes have been used for many decades to study samples in great detail. Their spatial resolution is much higher than that of optical microscopes due to the small de Broglie wavelength of electrons.

A traditional transmission electron microscope (TEM) uses high energy electrons, typically 30 kV to 300 kV, to obtain a very high resolution. However this is not a suitable method to study samples that are sensitive to radiation damage like graphene, polymer resists, DNA and proteins.

Recently Geelen et al. (2015) [1] developed a very low energy transmission electron microscopy technique called eV-TEM in which electrons arrive at the sample with an energy of only a few eV and the transmitted electrons are accelerated and imaged with an established aberration corrected low energy microscope imaging system [2].

Using low energy electrons ($<$100 eV) has the advantages of being able to perform measurements on samples sensitive to radiation damage, to directly measure the unoccupied bands of electron band structures [3] and to study low energy inelastic processes with high spatial resolution.

So far only graphene has been studied with eV-TEM. That is a simple sample, ideal to study and understand the technique with. Later more complicated samples are to be studied, which can be small particles deposited on graphene or several monolayers of different materials.

Here we present a new way of performing eV-TEM measurements on graphene, we determine the spatial resolution of eV-TEM and we investigate whether we can image something deposited on graphene with eV-TEM.

Chapter 2

Experimental methods

2.1 Sample preparation

In this section we describe the materials, equipment, machines and methods we use for sample preparation. The goal of the sample preparation is to find a way to deposit gold nanoparticles on graphene and ferritin on graphene in such a way the we can image those samples with LEEM and eV-TEM.

We used polished Si(100) wafer for initial experiments with gold nanoparticles. The goal of these experiments is to find out what happens when we deposit gold nanoparticles on a surface using different methods.

The graphene we use is a continuous film of 1–6 monolayers thick on a support film of lacey carbon. It is grown on nickel using chemical vapour deposition and transferred to a standard 300 mesh copper TEM grid with polymer-free transfer methods. The TEM grid has a typical graphene coverage of about 60 % to 90 %. We use the graphene to deposit gold nanoparticles or ferritin on it and to transfer the graphene from the TEM grid to a silicon nitride grid. The graphene was bought from Graphene Supermarket.

We use several solvents to clean glassware and samples: deionized type 1 water from Millipore (18.2 $M\Omega \cdot cm$ at 25 °C), acetone ($(CH_3)_2CO$) and isopropanol (C_3H_7OH or 2-propanol).

2.1.1 Gold nanoparticles

The gold nanoparticles were made by reduction of chloroauric acid ($HAuCl_4$) in type 1 water. Type 1 water, $HAuCl_4 \bullet 4H_2O$ (1%), citrate trisodium (1%), tannic acid (1%), ethanol (99%), isopropanol (70–100%), chloroform (99%) and laboratory equipment was used in the synthesis of the gold nanoparticles.

The gold nanoparticles solution was made by Sander Blok, Leiden University.

The gold nanoparticles are suspended in type 1 water with some trace acids from the synthesis process. The gold nanoparticles solution is diluted 10x with type 1 water from the starting solution. The gold nanoparticles are charge neutralized and have a diameter of $\approx$10 nm.

We use tweezers with a carbon tip to handle silicon and silicon nitride grids and inverted metal tweezers to handle TEM grids. Inverted tweezers are normally closed and can be opened by applying force to them.

We can deposit gold nanoparticles by touching silicon with the tip of a leg of tweezers from which a drop of gold nanoparticles solution is hanging.

Nebulizer

We can deposit gold nanoparticles by exposing a sample to the mist of a nebulizer containing the gold nanoparticles solution in the fume hood. The nebulizer creates and expels a mist of small droplets that precipitate on the sample and evaporate quickly at room temperature and ambient pressure.

Figure 2.1: *The nebulizer we use to deposit small droplets of gold nanoparticles solution on silicon and graphene*[*]*.*

We use the IH 50 nebulizer of Beurer GmbH, see figure 2.1. This nebulizer uses a double membrane with an oscillation frequency of 100 kHz to create and expel small droplets.

The droplets have a diameter of 2 µm to 40 µm with 50 % of the mass sum distribution at a diameter of 6 µm according to the specifications. We measured the diameter of the residue of a droplet of gold nanoparticles solution on Si(100) and its diameter was roughly 16 µm, see figure 3.4(b).

We use the nebulizer to deposit gold nanoparticles in two ways. For the first method we hold the sample vertically about 3 mm in front of the nebulizer using tweezers and then turn the nebulizer with gold nanoparticles solution on for a specific duration of time.

The second method is turning the nebulizer with gold nanoparticles solution on and moving the sample quickly past the exhaust of the nebulizer holding it with tweezers.

Cleaning equipment and samples

We use clean beakers and glass bottles. We clean glassware by rinsing it with acetone twice and then with isopropanol twice while blowing it dry with nitrogen gas after rinsing each time. Before use we rinse all glassware with the solvent we are going to put in it twice, blowing it dry with nitrogen gas after rinsing each time.

We clean silicon in an ultrasonic bath, first in acetone and then in isopropanol. We put the silicon in acetone in a beaker, place the beaker in an ultrasonic bath

[*]Source: `www.beurer.com/web/nl/products/nebulization/nebulization/IH-50`

and turn it on for 5 min. Afterwards we take the silicon out with tweezers, blow it dry with nitrogen gas and repeat the process with isopropanol instead of acetone.

We attempted to clean graphene with acetone and isopropanol by rinsing and dipping. This attempt has no positive effects as far as we can tell, see section 3.1.

Rinsing was done by holding the TEM grid with graphene with inverted tweezers, rinsing it with type 1 water, then rinsing it with acetone and finally rinsing it with isopropanol while carefully blowing it dry with nitrogen gas after rinsing each time.

Dipping was done by putting acetone and isopropanol in two beakers, holding the TEM grid with graphene with inverted tweezers, dipping the sample in acetone and then in isopropanol while carefully blowing it dry with nitrogen gas after dipping each time.

Pipette

We can deposit gold nanoparticles by putting a drop of gold nanoparticles solution on the sample with a pipette while we hold the sample in mid-air with inverted tweezers lying on a flat surface, see figure 2.2. The drop we put on the grid is large compared to the grid and would disperse over a larger area if the grid was lying on a surface.

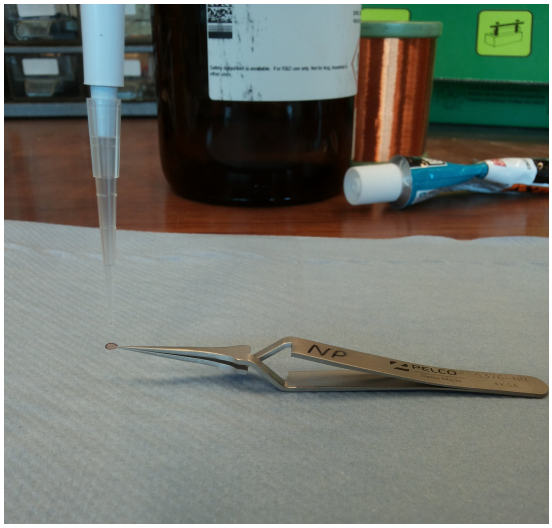

Figure 2.2: *Holding a TEM grid with graphene in mid-air and putting a drop on it with a pipette.*

Now we proceed in one of four ways. The first way is letting the drop evaporate in the fume hood at room temperature and ambient pressure. The second way is putting the sample in vacuum to speed up the evaporation. The third way is using a paper tissue after waiting a specified amount of time to suck up the drop. And the fourth way is sucking the drop up for the most part with a pipette after 10 s and sucking the remainder of the drop up with a paper tissue.

At first we used a large pipette that was calibrated for 100 µL to 1000 µL. Soon however we started to use a smaller pipette that is calibrated for 20 µL to 200 µL. The drops we deposit are around 16 µL, but this is not a problem, see section 4.1.

The first two drops of gold nanoparticles solution we deposited with a pipette was with the large pipette (method 14 and 15 of table 3.1). Hereafter we used the smaller pipette calibrated for 20 µL to 200 µL.

The vacuum we use to speed up evaporation is the load lock of a glove box. We use a plastic tray to put the inverted tweezers holding the TEM grid with the drop of gold nanoparticles solution in and place a foam over the edges of the tray to close off the tray and prevent air currents from blowing the drop of the TEM grid during pumping down or venting the vacuum chamber. The foam is held in place with a tie wrap and a rubber band.

Cleaning the gold nanoparticles solution

For later experiments we clean the gold nanoparticles solution by washing it twice. Washing means separating the gold nanoparticles from the solvent by centrifuging the gold nanoparticles solution at 10 °C and 1500 RPM for one hour, taking up the solvent with a pipette and adding the same amount of type 1 water. We placed 1.000 mL gold nanoparticles solution in several 1.5 mL disposable plastic tubes and placed them evenly distributed in the centrifuge. After centrifugation we moved the tubes carefully to the fume hood, took the solvent up with a pipette in several converging steps and added type 1 water such that the tubes contained 1 mL again.

After cleaning the gold nanoparticles solution, we diluted it to the desired concentration by adding type 1 water. We made 10 times diluted and 100 times diluted solution of gold nanoparticles.

After transferring graphene from a TEM grid to a silicon nitride grid as described in section 2.2, we deposit a drop of washed gold nanoparticles solution on it. We do this on a silicon nitride grid coated with chromium and tungsten with 10 times diluted washed gold nanoparticles solution.

2.1.2 Ferritin

We deposit a protein in solution on graphene with a pipette. We use ferritin from a horse spleen, which we buy from Sigma-Aldrich. The ferritin is dissolved in liquid and has a concentration of 10 mg/mL in 0.15 M NaCl. A ferritin molecule weighs 450 kDa so the ferritin concentration is 2.2×10^{-5} M.

We want to be able to look at individual proteins with LEEM and eV-TEM. Proteins clump together during deposition on a surface when their concentration is too high. Therefore we need to dilute the ferritin solution with an appropriate factor. We calculate this dilution factor using certain assumptions.

We calculate a dilution factor for depositing ferritin solution on graphene on a TEM grid assuming that we want to have one protein in a 500 nm $\times$ 500 nm area of graphene, that the proteins will be evenly dispersed over the TEM grid and that the drop we put on the TEM grid has a volume of 16 µL. For this we need a ferritin concentration of 2.9×10^{-12} M. The ferritin has a concentration of 2.2×10^{-5} M to start with so the dilution factor is 7.6×10^{6}.

One protein per 500 nm $\times$ 500 nm is not much so we also use higher concentrations of ferritin, see section 3.2.

We make several solutions with different ferritin concentration. First we put 15 mL type 1 water in a bottle and add 15 µL 2.2×10^{-5} M (undiluted) ferritin solution for a dilution of roughly 1000 times. Then we put 7.92 mL type 1 water in another bottle and add 80 µL 1000 times diluted ferritin solution for a dilution of roughly 10^5 times. Finally we put 6 mL type 1 water in a third bottle and add 80 µL 10^5 times diluted ferritin solution for a dilution of roughly 7.6×10^6 times.

We can deposit ferritin by putting a 16 µL drop of ferritin solution on the sample with a pipette calibrated for 20 µL to 200 µL. Now we proceed in one of two ways. The first way is letting the drop evaporate in the fume hood at room temperature and ambient pressure. The second way is using a paper tissue to suck up the drop after waiting 30 s. For some samples this procedure is repeated twice.

2.1.3 Machines and software

We use a digital optical microscope in a cleanroom to look for contaminants and large structures on our samples and to look at the graphene coverage on TEM and silicon nitride grids and to take pictures of this. This microscope has a magnification ranging from 50 to 1000 times.

We use the FEI NanoSEM 200 to check the amount of gold nanoparticles or ferritin molecules and their dispersion on our samples. This Scanning Electron Microscope (SEM) is a Schottky field emitter SEM that produces images of a sample by scanning it with a focused beam of electrons.

Settings we use for graphene with gold nanoparticles are:

- An accelerating voltage of 2 kV when we want to have good contrast on graphene and 5 kV when we want to have good contrast on gold nanoparticles while still being able to see the graphene.
- A small working distance of ≈3 mm.
- A small (high number (5.0)) spot size
- For ferritin we use an accelerating voltage of 2 kV.

We use the JPK NanoWizard AFM to check the amount of ferritin molecules and their dispersion on our samples and to check the flatness of graphene on a TEM grid.

A cantilever with a resonance frequency of ≈240 kHz is used. We use a line rate (the number of lines scanned per second) of 1.5 Hz to scan a small area of 306 nm × 306 nm, of 1.0 Hz to scan medium sized areas of 1 µm × 1 µm and 5 µm × 5 µm and of 0.4 Hz to scan a large area of 15 µm × 15 µm.

We use Gwyddion to process images made with the AFM.

With Gwyddion we can level AFM images using different algorithms, e.g. mean plane subtraction and flatten base (for flat surfaces with a number of large features), shift the values of the measured parameter and exclude certain regions of the image from these processes. With Gwyddion we can also make line scans and save the height profiles.

Version of 18-08-2016– Created August 18, 2016 - 11:48

2.2 Flatter graphene on a silicon nitride grid

We want to make a sample with flatter, less wrinkled graphene to make working with graphene with eV-TEM easier and less time consuming. For that purpose we transfer graphene from a TEM grid to a silicon nitride grid.

The silicon nitride grids are circular disks with a diameter of $3.00 \pm 0.05\,\text{mm}^{\dagger}$ consisting of $200 \pm 15\,\mu\text{m}^{\dagger}$ thick silicon and a $200 \pm 10\,\text{nm}^{\dagger}$ thin layer of silicon nitride (Si_3N_4) on one side. In the middle of the grid is a $0.32\,\text{mm} \times 0.32\,\text{mm}$ square of 200 nm thick silicon nitride without silicon underneath. In this square an array of holes with a diameter of 2.5 µm is made.

We have used grids with holes in the whole square thin part and grids with holes in only a small part of the square thin part. The grids with holes in the whole square thin part should be used. See figure 2.3 for a cross section (not to scale) including the thin square in the middle of a silicon nitride grid after a conductive coating is applied.

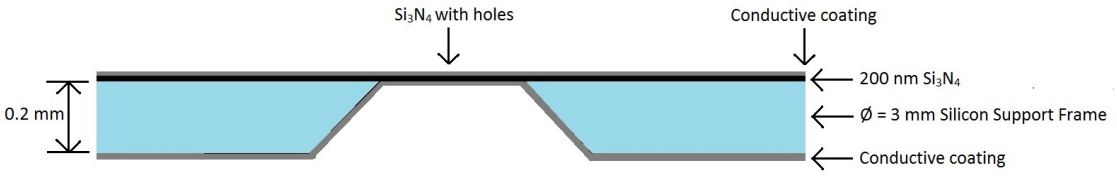

Figure 2.3: *Cross section of the silicon nitride grid with a conductive layer on both sides. The thin only silicon nitride part in the middle is the area with holes in it. Light blue: silicon, black: silicon nitride, grey: conductive coating.*

Conductive coating

Silicon nitride is not a good electrical conductor and in order to prevent charging effects during eV-TEM measurements, the silicon nitride grids need a conductive coating on both sides. We coat separate grids with three different conductive layers: chromium, tungsten on top of chromium and titanium.

We consider two things in choosing the material of the conductive layer. Firstly we need to be able to transfer a good amount of graphene to the coated grid and secondly the conductive layer should not break off when the grid is heated.

Layers of different materials can separate during heating when one expands more than the other due to a difference in thermal expansion coefficients. So we select metals with thermal expansion coefficients close to that of silicon nitride.

[†]Source: `www.tedpella.com/grids_html/silicon-nitride-details.htm`

Version of 18-08-2016– Created August 18, 2016 - 11:48

We apply the coating by sputter deposition. In sputtering a target material is bombarded with energetic gas ions, which eject particles from the target. These particles are then accelerated to the sample and form a thin film on the sample. We use a Z-400 sputtering system of Leybold Heraeus to sputter the conductive layer.

The three conductive layers on separate grids are 50 nm chromium, 20 nm tungsten on top of 10 nm chromium and 30 nm titanium. We sputter an adhesive layer of chromium before sputtering the tungsten because tungsten does not adhere well to silicon nitride. A thick layer breaks off more easily during heating so we want to sputter a thin layer, but the conductive layer needs to be thick enough to be fully closed.

The silicon nitride grids need to be handled carefully. The 200 nm thick silicon nitride square is fragile and trying to clean the grid might result in the thin square breaking off. Therefore we transfer the graphene in the cleanroom as soon as possible after the conductive layer is sputtered.

Graphene transfer

We used two methods of transferring graphene from a TEM grid to a silicon nitride grid. The first one is a variation of a method from Pantelic et al. (2011a) [4] and Algara-Siller et al. (2014a) [5]. The second one is from Pantelic et al. (2011a) [4].

Method one is applying some isopropanol to a silicon nitride grid, putting the TEM grid with graphene on it and letting the isopropanol evaporate at room temperature and ambient pressure. Method two is applying some chloroform to a silicon nitride grid, putting the TEM grid with graphene on it, heating the grids to $\approx$200 °C and keeping it at that temperature for roughly 5 min.

The drying agent (isopropanol or chloroform) is in contact with both the graphene and the silicon nitride grid and as it evaporates, the graphene is pulled into close contact with the silicon nitride grid, after which the graphene sticks to the grid.

In this procedure, both grids can be in two orientations. The silicon nitride grid should have the silicon nitride layer on top, the drying agent applied on the coated silicon nitride layer and the TEM grid be put on the drying agent with the graphene facing down.

Afterwards the TEM grid is removed and freestanding graphene has been transferred to the coated silicon nitride grid if the transfer was successful.

2.3 ESCHER

We use the cathode lens microscope called ESCHER to image freestanding graphene with and without gold nanoparticles with low energy electrons. ESCHER consists of a sample, an imaging system and an illumination system.

The imaging system accelerates low energy electrons from a sample and guides them to a detector. Three different illumination systems can be combined with the imaging system: PEEM, LEEM and eV-TEM.

Low energy electron microscopy (LEEM) uses low energy electrons reflected from a surface for making an image of a surface. Photo emission electron microscopy (PEEM) uses ultraviolet light to eject electrons from the sample. Very low electron energy transmission electron microscopy (eV-TEM) sends low energy electrons to the backside of a thin sample in order to make an image of the transmitted electrons.

First we describe the imaging system, then the illumination systems, the general procedure for aligning the imaging system and finally we briefly describe how we use LEEM or eV-TEM to make an image of a sample.

For a schematic view of the instrument (with all deflectors and stigmators but without PEEM and eV-TEM) see figure 2.4(a).

Imaging system

The imaging system is the part of the microscope that accelerates the low energy electrons away from the sample and guides the electrons from the sample via a series of electromagnetic lenses, two magnetic prism arrays (MPA's) and an electron mirror to the detector. The electrons have a high energy of 15 keV to minimise chromatic aberrations in the imaging system.

The electrons that are emitted, reflected or transmitted by the sample are accelerated by the potential difference between the sample at -15 keV and the grounded objective lens (OL). The objective lens focuses the electron beam and the transfer lens (TL (M1 in figure 2.4(a))) focuses the diffraction pattern.

The magnetic prism arrays deflect the electron beam by 90° from the LEEM gun to the sample (only for LEEM), from the sample to the electrostatic lens (EL), from EL to the electron mirror and from the mirror to the detector.

Version of 18-08-2016– Created August 18, 2016 - 11:48

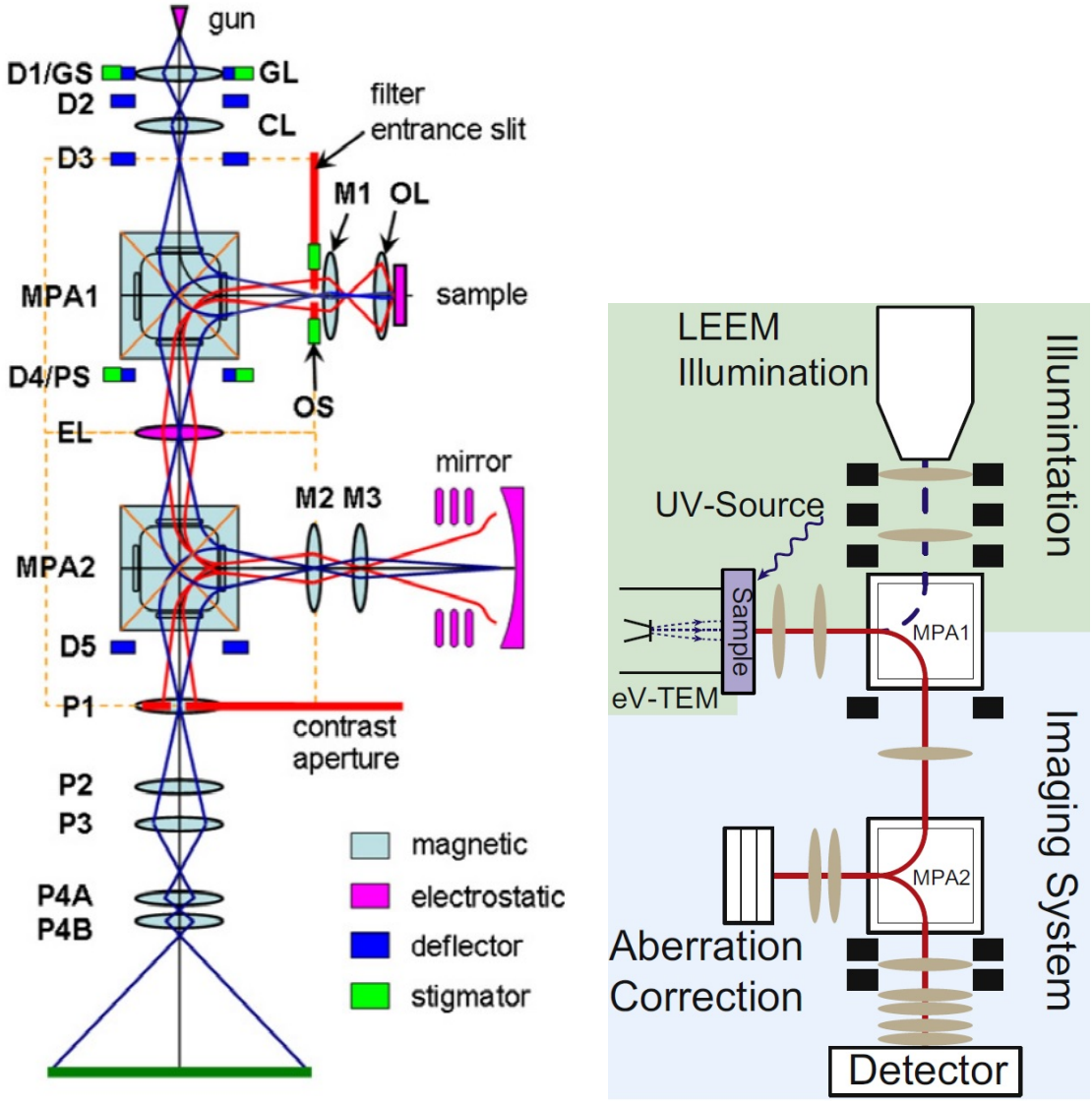

(a) ***(b)***

Figure 2.4: *(a) A schematic view of ESCHER including all deflectors and stigmators. The only illumination system shown is LEEM. Source: [6]. (b) A schematic view of ESCHER showing all three possible illumination systems. Source: [1]*

A series of electromagnetic lenses, deflectors and stigmators is used to transfer the virtual images and diffraction patterns to the correct positions and finally to the detector.

The detector consists of a channelplate-intensified phosphor screen and a cooled Sensicam CCD camera [6].

The electron gun, lenses, prisms, sample chamber, electron mirror and detector are all held at ultra-high vacuum because the mean free path of the electrons needs to be long enough for the electrons to reach the sample and the detector. Imaging, with temperatures between room temperature and several hundred degrees Celsius, is normally performed with a pressure in the sample chamber below 2×10^{-9} mbar to prevent arcing between the sample and the objective lens.

The LEEM electron gun has three ion pumps, both MPA's have an ion pump, which also pump the transfer lens and the electron mirror via bypasses. The sample chamber has a turbomolecular pump, an ion pump and a titanium sublimation pump. The load lock and the transfer room used to insert samples in the microscope have a turbomolecular pump and an ion pump respectively. The detector has an ion pump [6].

The electron mirror consists of four silicon-bronze discs, spaced with polyether ether ketone (PEEK). The first electrode is at ground potential, the next three electrodes are held at increasingly negative potentials. With three independently controllable parameters the focal length of the mirror, the spherical aberrations C_3^m and the chromatic aberrations C_c^m of the mirror can be independently set [2, 6].

The electron mirror can correct the spherical C_3 and chromatic C_c aberrations of the imaging system, but no higher order aberrations.

For more details about the working of the electron mirror see appendix B.

Version of 18-08-2016– Created August 18, 2016 - 11:48

Illumination system

With PEEM we bombard the sample with ultraviolet light from a Hg discharge lamp and image photoelectrons. PEEM has a lower resolution than LEEM. We use PEEM only for aligning the imaging system when we want to have signal from a large area of the sample.

With LEEM the electrons are extracted from a filament in the gun and guided to the sample by a magnetic prism array and magnetic lenses. A cold field emission gun emits a beam of electrons at 15 keV electron energy and ≈250 meV energy width [6].

The sample is kept at a high negative potential that decelerates the incoming electrons. The landing energy is determined by the potential difference between the electron gun cathode and the sample. The electrons interact with the sample with an energy of typically 0 eV to 100 eV and are accelerated back to the objective lens.

For eV-TEM a BaO coated tungsten disc cathode is located behind the sample in the sample holder. The cathode emits an electron beam at 15 keV and ≈800 meV energy width. The electrons emitted by the cathode are guided to the sample and the electron landing energy is determined by the potential difference between the cathode and the sample. A thin sample that is transparent to electrons is needed for eV-TEM. The electrons that go through the sample are accelerated by the sample at a high potential towards the objective lens [1].

For a schematic view of the instrument including eV-TEM see figure 2.4(b).

Several measures to minimise the effects of external vibrations have been taken in designing the microscope. ESCHER has an active vibration isolation system (Herzan AVI-400) [6].

ESCHER has retractable apertures and grids at several positions. They are used as alignment tools and to improve image quality.

The diagonals of the MPA's and the centre planes of the magnetic transfer lenses (MTL1 and MTL2 (M2 and M3 respectively in figure 2.4(a))) have retractable apertures of various diameters, as well as conventional TEM grids and PELCO grids. TEM grids have an array of approximately 50 µm × 50 µm square holes and PELCO grids have an array of 2.5 µm diameter circular holes.

An energy filter slit is located at the entrance plane of MPA1 and a contrast aperture is located in the centre of magnetic transfer lens P1, which can be used to

block all electrons that did not leave the sample perpendicularly. Both increase image quality and can be used to perform energy filtered measurements [2].

Alignment

Alignment is done in several iterations, making the alignment better with each iteration. Making the electron mirror temporarily flat so it does not correct aberrations makes the alignment easier. If the mirror is not flat, a slightly off-axis incidence at the electron mirror causes large aberrations.

An alignment iteration consists of placing the image plane at the correct position and minimising astigmatism in that image plane for the image planes in consecutively the bottom diagonal of MPA2, the centre of MTL1 after reflection by the mirror, the centre of MTL1 before reflection by the mirror, the top diagonal of MPA2 and the bottom diagonal of MPA1.

We place an image plane at the correct position by inserting a TEM grid or a PELCO grid where the image plane should be, defocusing the sample so only the grid is in focus and focusing on the grid using either PEEM or LEEM. When we use LEEM we use mirror mode, which means the landing energy is negative so the electrons do not touch the sample. We use mirror mode because then the electron beam does not suffer from interaction with the sample.

We temporarily change the focus of the electron mirror while looking at the image plane in MTL1 after reflection, so the TEM grid in MTL1 before reflection is always out of focus.

If the alignment of the imaging system is not close to optimal yet, reducing astigmatism is easiest by trying to make the holes of the grid square or circular (for a TEM grid or a PELCO grid respectively) and using PEEM to look at a large area. We use the PELCO grids in the diagonals and LEEM at high magnification to optimise the alignment because LEEM has a smaller field of view and the holes in a PELCO grid are much smaller than in a TEM grid. Optimising the alignment requires a high magnification or else the pixel size of the detector becomes the limiting factor.

We minimise astigmatism by looking at the lattice of the circular holes of the PELCO grid. The circles should form a hexagonal lattice. We draw a line between adjacent holes and the line that should be perpendicular to it between two other adjacent holes. We can do this in three different directions and make the angles of the lines as close to 90° as possible.

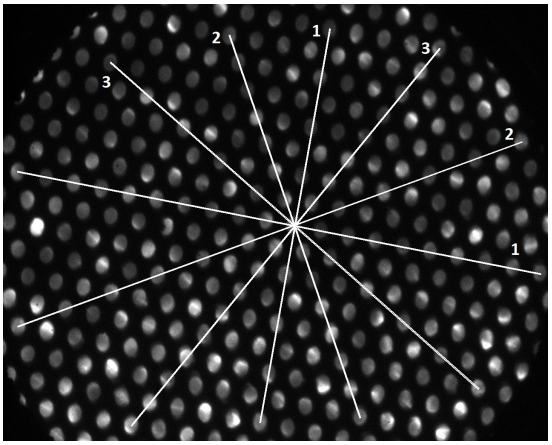

Figure 2.5: *PELCO grid in a diagonal of a MPA. In three directions lines between adjacent holes and the lines that should be perpendicular to them are drawn.*

See figure 2.5 for an example of what a PELCO grid in a diagonal of a MPA looks like. The circles should form a hexagonal lattice. Angle 1, the angle between the two lines numbered 1, is $90.99 \pm 0.01°$, angle 2 $88.82 \pm 0.01°$ and angle 3 $87.85 \pm 0.01°$. Here the total deviation from three perfect 90° angles is $4.32 \pm 0.03°$.

For more details about the alignment procedure see appendix B.

Imaging

A sample can be cleaned by heating it to temperatures around 1000 °C. We clean the samples we use for aligning to create a very clean surface. We do not heat our samples after we have deposited something on it because heating destroys those samples.

A high quality image is only formed when the electrons travel from the gun to the sample and from the sample to the detector under the correct conditions. For this we need to focus the electrons emitted by the gun and correct for astigmatism of the gun lens (only for LEEM), correct sample tilt so either the incidence of the electrons on the sample is perpendicular (for LEEM) or the surface of the sample is perpendicular to the objective lens (for eV-TEM), focus the electrons from the sample and correct astigmatism of the objective lens and set the incidence of the electron beam at the mirror perpendicularly.

Finally we use the energy filter slit and the contrast aperture to block all electrons that did not leave the sample perpendicularly with the desired energy.

Chapter 3

Results

3.1 Gold nanoparticles deposition

In this section we show the results of our experiments with depositing gold nanoparticles on silicon and on graphene. We want to deposit gold nanoparticles on graphene in such a way that we can image them with LEEM and eV-TEM.

We expect the coffee ring effect to complicate depositing gold nanoparticles. The coffee ring effect leads to the aggregation of gold nanoparticles, which makes it impossible to image (part of) the sample with eV-TEM, see Deegan et al. (1997) [7] and Askounis et al. (2015) [8] for more information about the coffee ring effect. In order to study the occurrence of the coffee ring effect in an evaporating drop of gold nanoparticles solution on graphene we looked at droplets of gold nanoparticles solution that were deposited on silicon and graphene with different methods.

Table 3.1 summarizes the various gold nanoparticles deposition methods and whether we observed the coffee ring effect or not. From now on we refer to the methods in table 3.1 when using method numbers.

We start by showing what silicon and graphene on a TEM grid look like without depositing anything on it in order to be able to determine the effect of depositing something on it. We have four control samples: uncleaned silicon (control 1), cleaned silicon (control 2), uncleaned graphene on a TEM grid (control 3) and 'cleaned' graphene on a TEM grid (control 4).

Table 3.1: *Gold nanoparticles deposition methods. 'Deposition' denotes the instrument used for deposition. 'Surface' denotes the surface on which the gold nanoparticles solution was deposited. 'Dose' denotes the duration of exposure to the mist of the nebulizer or deposition method FP (Fast Pass, meaning the sample was quickly moved past the exhaust of the turned on nebulizer) or SO (Short On, meaning the nebulizer was turned on and off quickly with the sample in front of the exhaust) or the volume used to deposit the gold nanoparticles using a pipette. 'Cleaned' denotes whether the surface was cleaned before deposition or not. 'Evaporation' denotes whether and how the gold nanoparticles solution evaporated. 'CRE' denotes whether the coffee ring effect was observed or not.*

Method	Deposition	Surface	Dose	Cleaned	Evaporation	CRE
1	Tweezers	Silicon	Large	No	Normal	Yes
2	Nebulizer	Silicon	5 s	No	Normal	Yes
3	Nebulizer	Silicon	30 s	No	Normal	Yes
4	Nebulizer	Silicon	FP	No	Normal	
5	Nebulizer	Silicon	SO	No	Normal	
6	Nebulizer	Silicon	FP	Yes	Normal	
7	Nebulizer	Silicon	5 s	Yes	Normal	Yes
8	Nebulizer	Silicon	SO	Yes	Normal	Yes
9	Nebulizer	Graphene	FP	No	Normal	
10	Nebulizer	Graphene	FP	Yes[a]	Normal	
11	Nebulizer	Graphene	FP	Yes[a]	Normal	
12	Nebulizer	Graphene	10 s	No	Normal	
13	Nebulizer	Graphene	90 s	No	Normal	
14	Pipette	Graphene	15 µL	No	Tissue	
15	Pipette	Graphene	16 µL[b]	No	Normal	
16	Pipette	Graphene	16 µL[b]	No	Normal	Yes
17	Pipette	Graphene	16 µL	No	Vacuum	Yes
18	Pipette	Graphene	6 µL	No	Normal	

[a] Methods 10 and 11 use different cleaning methods.
[b] In contrast to method 15 the dose of method 16 was measured instead of estimated.

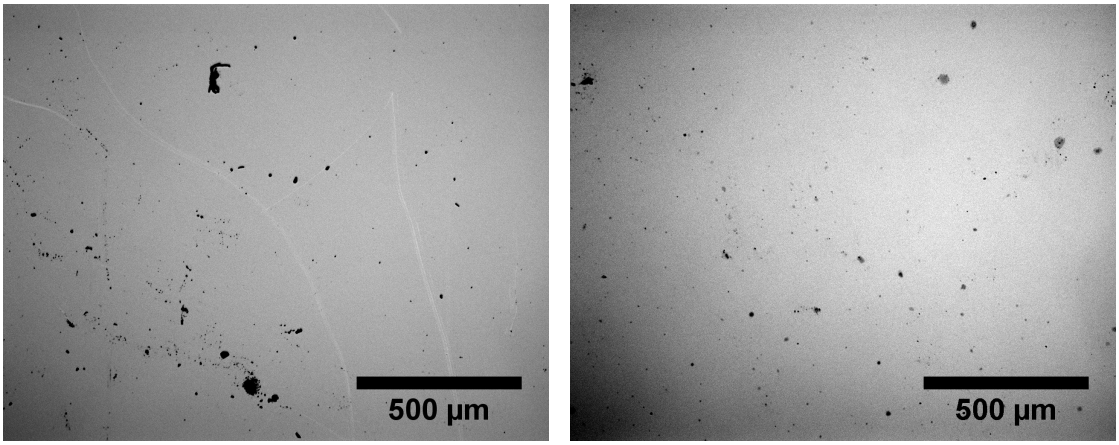

(a) ***(b)***

Figure 3.1: *Optical microscope images of control samples of (a) uncleaned and (b) cleaned silicon. (a) shows a lot of contamination on the silicon and (b) also shows a lot of contamination of the silicon, but (b) has no large contaminants and is somewhat cleaner than (a). (b) is cleaned in an ultrasonic bath, first in acetone and then in isopropanol.*

The silicon control samples (control 1 and 2) have a lot of large contaminants on the surface, both the uncleaned silicon, see figure 3.1(a), and the cleaned silicon, see figure 3.1(b). The silicon is cleaned in an ultrasonic bath, first in acetone and then in isopropanol.

The graphene control samples (control 3 and 4) can be seen in figure 3.2. The low (figure 3.2(a)) and high (figure 3.2(b)) magnification optical microscope images show a TEM grid with graphene before deposition and without cleaning it. The SEM image seen in figure 3.2(c) shows what the graphene looks like before deposition. Figure 3.2(d) shows a cleaned TEM grid with graphene before deposition (method 4). The sample was cleaned by rinsing it with acetone and isopropanol. Compared to uncleaned graphene, cleaning graphene leaves residue of either aceton or isopropanol or both on the sample, which is mainly seen on the bars of the copper TEM grid. We see no evidence of the cleaning procedure on freestanding graphene.

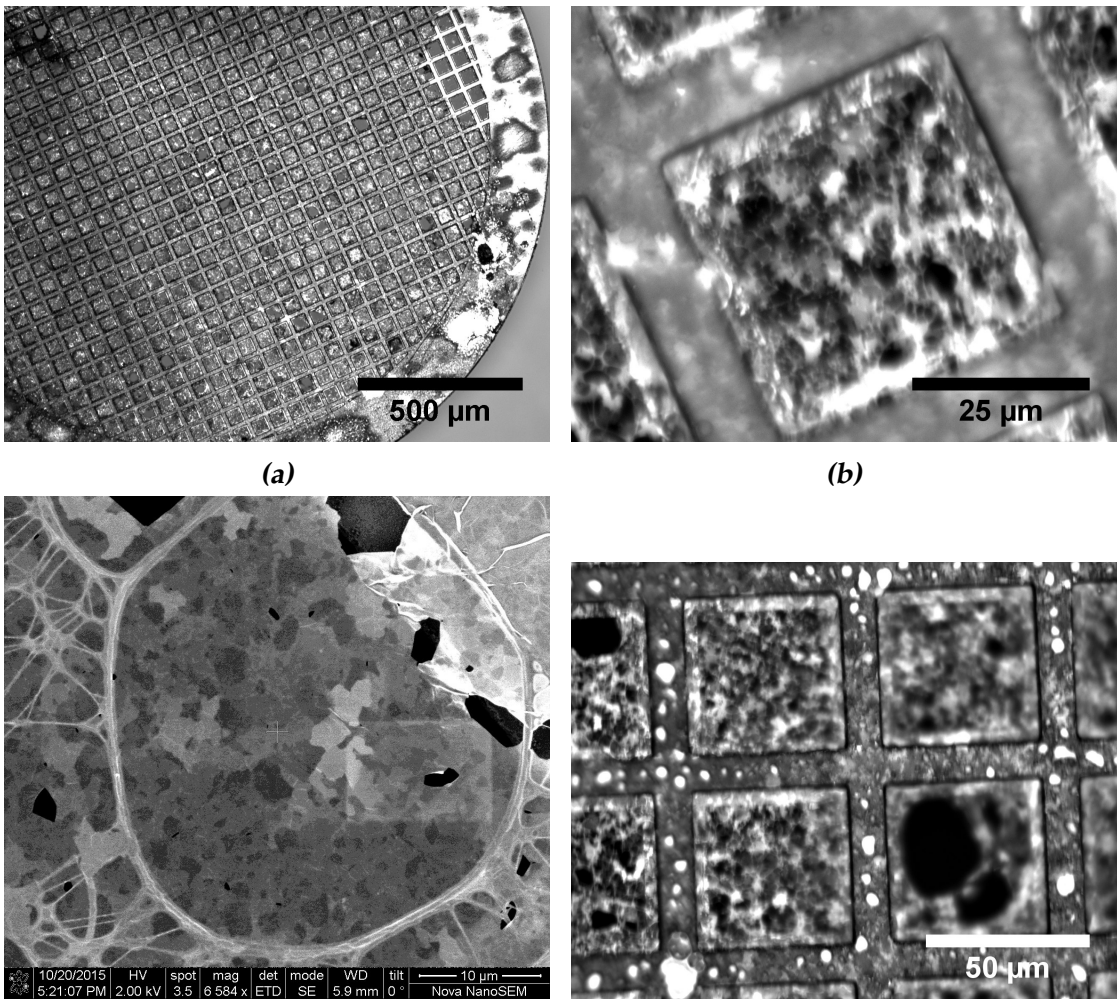

(a) ***(b)*** ***(c)*** ***(d)***

Figure 3.2: *Optical microscope images at (a) low and (b) high magnification of a control sample of uncleaned graphene on a TEM grid. (c) SEM image by Daniël Geelen of graphene on a TEM grid, which serves as a control sample. (d) Optical microscope image of a control sample of cleaned graphene on a TEM grid.*

Tweezers

Gold nanoparticles deposition method 1 (depositing a big drop of gold nanoparticles solution that was hanging from tweezers on silicon, which was allowed to evaporate under atmospheric conditions) gives a clear example of the coffee ring effect of gold nanoparticles solution on silicon, see figure 3.3.

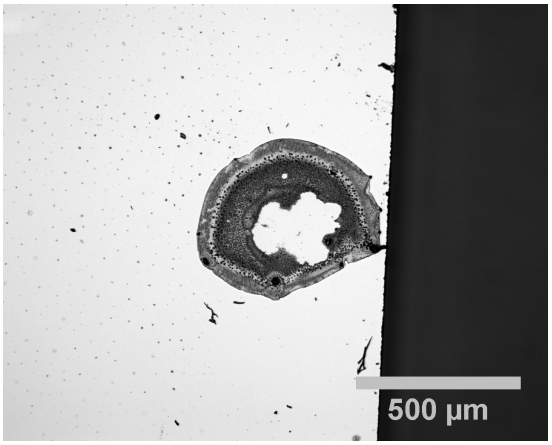

Figure 3.3: *Optical microscope image of a gold nanoparticles ring on the edge of uncleaned silicon as a result of the coffee ring effect during the evaporation of a deposited big drop of gold nanoparticles solution hanging from tweezers (method 1).*

Nebulizer

We start with depositing small droplets of gold nanoparticles solution with the nebulizer because we expect to suffer from the coffee ring effect if we use large drops.

Uncleaned silicon that is exposed to the mist of the nebulizer with gold nanoparticles solution for 5 s (method 2) is covered with nested ring-like structures resulting from the coffee ring effect as can be seen in figure 3.4. Figure 3.4(b) is zoomed in at one of the coffee ring structures in figure 3.4(a) and the original size of the droplet on the silicon is clearly visible. The diameter of the droplet on the silicon in figure 3.4(b) is 15.9 µm.

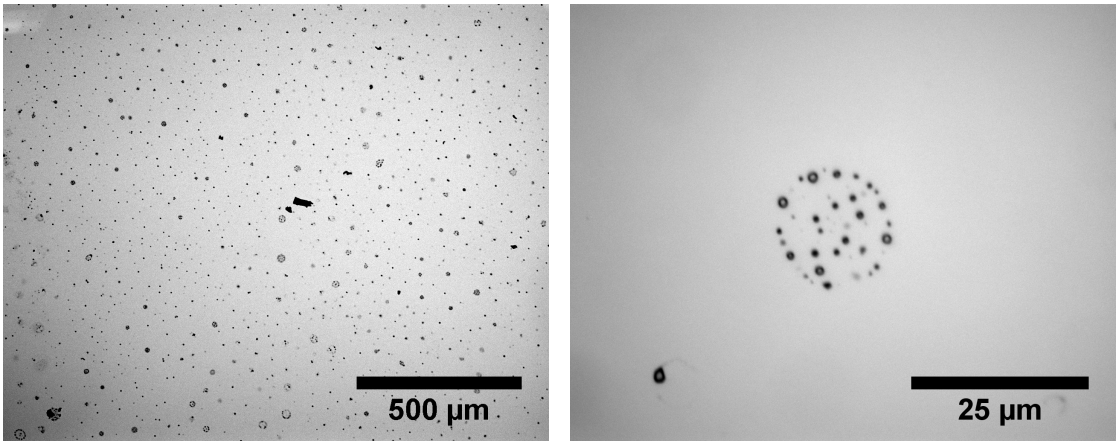

(a) **(b)**

Figure 3.4: *(a) Low and (b) high magnification optical microscope images of gold nanoparticles on uncleaned silicon after* 5 s *exposure to gold nanoparticles mist (method 2).*

The coffee ring structures are bigger and more pronounced when we expose uncleaned silicon to the gold nanoparticles mist for 30 s (method 3), see figure 3.5. These optical microscope images show large and small coffee ring structures all over the silicon. If the droplets are sprayed on the silicon faster than they evaporate, droplets agglomerate and bigger coffee ring structures form.

We did not clean the silicon, so a lot of contaminants sit on the surface. The structures we see in figures 3.3, 3.4 and 3.5 are not contaminants as they are not observed in the control samples seen in figure 3.1.

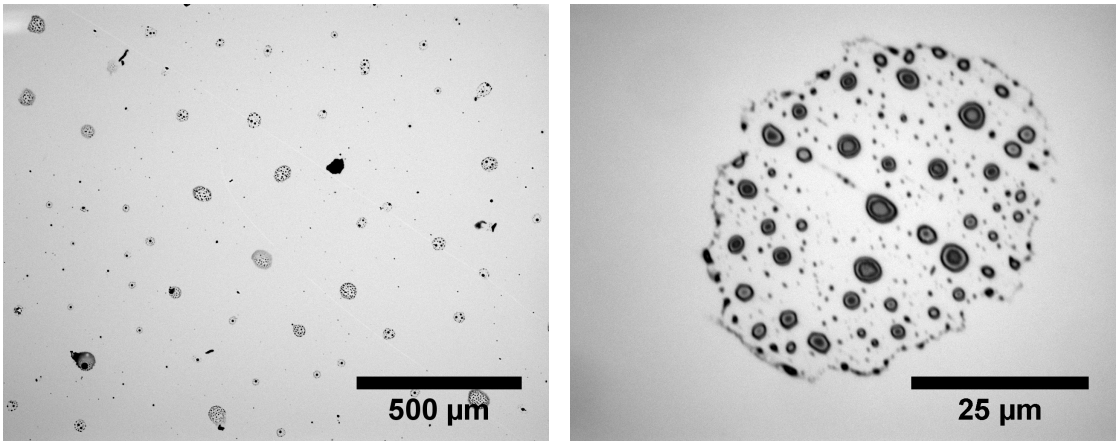

(a) **(b)**

Figure 3.5: *(a) Low and (b) high magnification optical microscope images of gold nanoparticles on uncleaned silicon after* 30 s *exposure to gold nanoparticles mist (method 3) with mostly large coffee ring structures and some smaller ones.*

Methods 4 and 5, which are exposing uncleaned silicon to the lowest possible dose of gold nanoparticles mist, do not give rise to a coffee ring effect observable with the optical microscope. Method 4 is moving the sample quickly past the exhaust of the turned on nebulizer and method 5 is turning on and off the nebulizer quickly with the sample in front of the exhaust.

Samples are usually cleaned before being used, but this might alter the coffee ring effect so we investigate both cleaned and uncleaned silicon in the hope that this will give an indication of the effect that cleaning graphene might have on the coffee ring effect.

Method 6 also does not give rise to a coffee ring effect observable with the optical microscope. Method 6 is exposing cleaned (in an ultrasonic bath, first in acetone and then in isopropanol) silicon to the lowest possible dose of gold nanoparticles mist by moving the sample quickly past the exhaust of the turned on nebulizer.

Method 7 (silicon, cleaned in an ultrasonic bath, first in acetone and then in isopropanol, and exposed to gold nanoparticles mist for 5 s) results in some coffee ring structures near the four edges of the cleaned silicon and no coffee ring structures that are visible with an optical microscope on the bulk of the cleaned silicon, see figures 3.6(a).

With the SEM we can see coffee ring structures everywhere on the cleaned silicon made with method 7, but they are smaller in size than the coffee ring structures on uncleaned silicon, see figure 3.6(b).

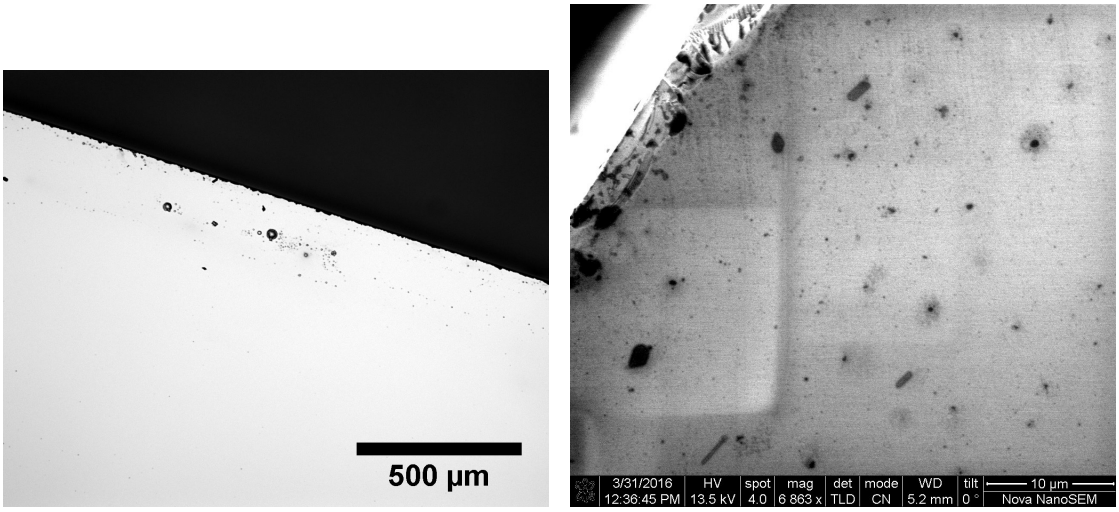

(a) ***(b)***

Figure 3.6: *(a) Optical microscope image and (b) SEM image of gold nanoparticles on cleaned (in an ultrasonic bath, first in acetone and then in isopropanol) silicon after* 5 s *exposure to gold nanoparticles mist (method 7). near an edge of the silicon. In (a) we see some coffee ring structures only near the edges of the silicon, while in (b) several medium sized and smaller coffee ring structures and contaminants are visible.*

Cleaning the silicon makes the coffee ring effect weaker and the coffee ring structures smaller and less pronounced, compare methods 2 (uncleaned silicon) and 7 (cleaned silicon), which have the same 5 s exposure to gold nanoparticles mist.

We see an even weaker coffee ring effect using method 8 (cleaned silicon, in an ultrasonic bath, first in acetone and then in isopropanol, that is held in front of the exhaust of the nebulizer, which is turned on for a very short time) than using method 7 (5 s of gold nanoparticles mist on cleaned silicon). The bulk of the cleaned silicon has no coffee ring structures on it that are visible with an optical microscope and only near the edges very few coffee ring structures are observed.

Method 9 does not give rise to a coffee ring effect observable with the optical microscope. Method 9 is exposing uncleaned graphene to the lowest possible dose of gold nanoparticles mist by moving the sample quickly past the exhaust of the turned on nebulizer

Cleaning graphene on a TEM grid leaves residue of the cleaning agent(s) on the bars of the TEM grid, but using the optical microscope we did not see any evidence on freestanding graphene of either the cleaning or the deposition of gold nanoparticles after having used the fast pass deposition method (moving

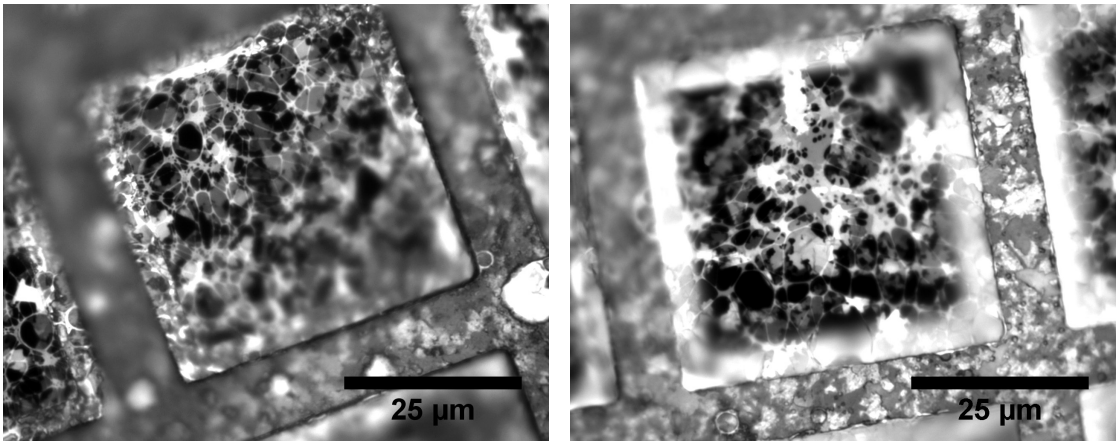

(a) ***(b)***

Figure 3.7: *Optical microscope images of cleaned graphene after the graphene was moved quickly past flowing gold nanoparticles mist. (a) was cleaned by rinsing the TEM grid with graphene with acetone and isopropanol (method 10). (b) was cleaned by dipping the TEM grid with graphene in acetone and isopropanol (method 11). (b) and especially (a) show residue of the cleaning agent(s) on the bars of the TEM grid, but no evidence of the cleaning or the deposition on the freestanding graphene can be observed with the optical microscope.*

the graphene quickly past the exhaust of the turned on nebulizer).

Methods 10 and 11 use the fast pass deposition method, but method 10 is rinsing the graphene with acetone and isopropanol first, see figure 3.7(a), and method 11 is dipping the graphene in acetone and isopropanol first, see figure 3.7(b).

We did not use the SEM to look at the samples made with methods 9, 10 and 11 so no data about the presence of gold nanoparticles on the graphene can be presented.

Using method 12 the bulk of the graphene has no gold nanoparticles on it except for a few concentrated groups of gold nanoparticles resulting from an evaporated droplet of gold nanoparticles solution, see figure 3.8(a) for such a group of gold nanoparticles. Method 12 is graphene on a TEM grid after 10 s exposure to gold nanoparticles mist.

Using method 13 the freestanding graphene is covered with reasonably spaced individual gold nanoparticles or small groups of gold nanoparticles, see figure 3.8(b). Method 13 is graphene on a TEM grid after 90 s exposure to gold nanoparticles mist.

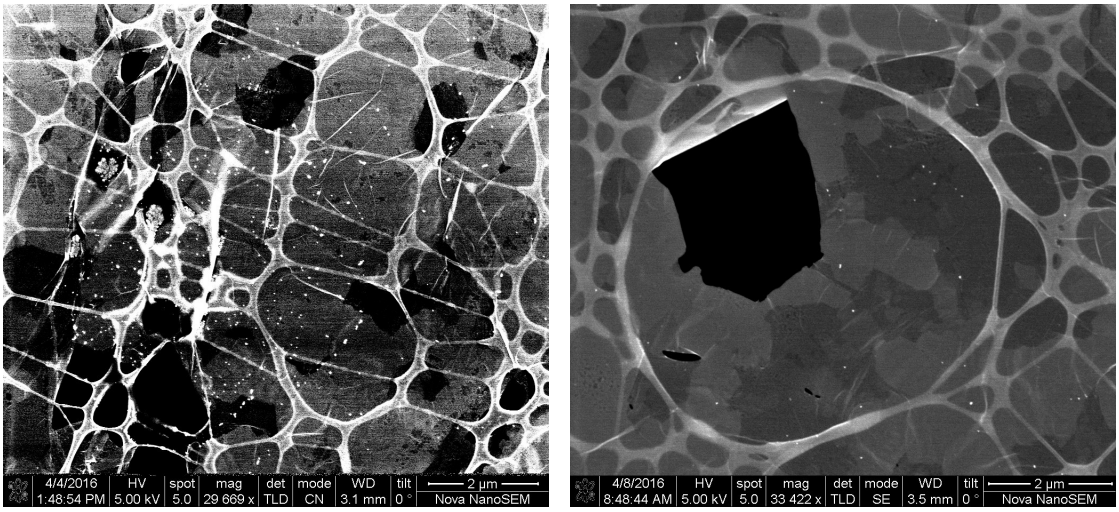

(a) ***(b)***

Figure 3.8: *SEM images of graphene on a TEM grid after (a)* 10 s *(method 12) and (b)* 90 s *(method 13) exposure to gold nanoparticles mist. (a) Zoomed in at one of only a few droplets of gold nanoparticles present using method 12. (b) A typical image of the dispersion of gold nanoparticles on freestanding graphene using method 13 with some individual and small groups of gold nanoparticles.*

Exposing graphene to gold nanoparticles mist from the nebulizer neither gives rise to the coffee ring effect nor deposits a lot of gold nanoparticles on graphene, no matter whether 10 s exposure (method 12), 90 s exposure (method 13) or the fast pass deposition method is used.

Pipette

In order to increase the amount of gold nanoparticles on the graphene we use a pipette to deposit drops on the graphene on a TEM grid that are very large compared to the droplets from the nebulizer. For method 14 we deposit a drop of 15 ± 10 µL on graphene on a TEM grid with a pipette, suck it up for the most part with a pipette after 10 s and suck the remaining solution up with a paper tissue. The amount of gold nanoparticles on freestanding graphene is very low using method 14.

Using method 15 results in a good dispersion of gold nanoparticles on freestanding graphene, with both individual gold nanoparticles and small groups of gold nanoparticles on the graphene. This typically looks like figure 3.9(a). When we take a closer look like in figure 3.9(b) we see that the gold nanoparticles mostly sit next to each other on the graphene and only a small portion

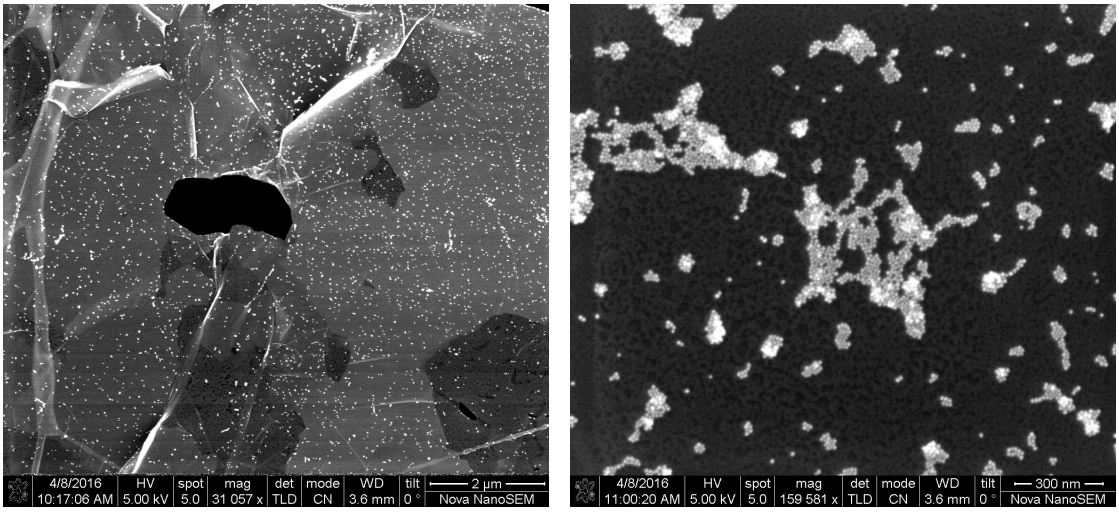

(a) ***(b)***

Figure 3.9: *(a) Medium and (b) high magnification SEM images of freestanding graphene after putting a drop of* $15 \pm 5\,\mu L$ *on a TEM grid with graphene and letting it evaporate (method 15). (a) shows a nice dispersion of indivual and small groups of white spots, which are gold nanoparticles, on the graphene. (b) is more zoomed in on another part of the graphene and indivual gold nanoparticles and structures of gold nanoparticles are clearly visible. We see that the gold nanoparticles mostly sit next to each other on the graphene and only a small portion of the gold nanoparticles sit on other gold nanoparticles.*

of the gold nanoparticles sit on other gold nanoparticles. No coffee ring effect is observed using method 15. Method 15 is putting a drop of $15 \pm 5\,\mu L$ on a TEM grid with graphene and letting it evaporate in the fume hood under atmospheric conditions.

To check whether the white spots observed in figure 3.9 are really gold nanoparticles we look at an individual gold nanoparticle and measure its diameter in the horizontal direction with a line scan of 3 pixels wide, see figure 3.10. The brightness and contrast of the SEM for the SEM image of figure 3.10(a) is set such that the graphene is not visible and the gold nanoparticles are not saturated. Figure 3.10(b) shows the line scan of the encircled gold nanoparticle of figure 3.10(a). The FWHM of the line scan is $12.0 \pm 0.2\,nm$. The line scan is 3 pixels wide to minimise the effects of noise.

Using method 16 the majority of the squares of the TEM grid look the same as with method 15 and have a good dispersion of gold nanoparticles on the graphene without big clusters of gold nanoparticles, but we observe deviating structures on part of the sample.

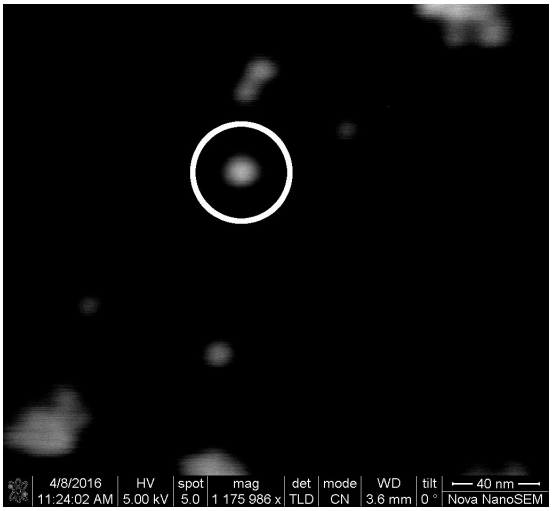

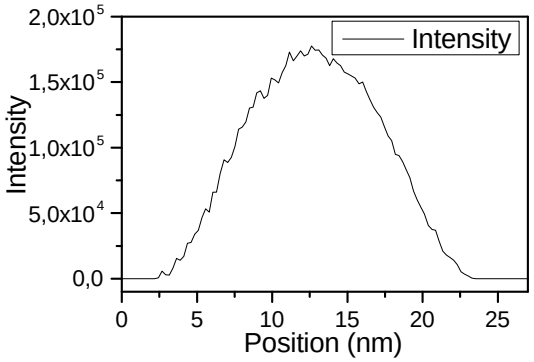

(a) ***(b)***

Figure 3.10: *(a) Very high magnification SEM image of gold nanoparticles on freestanding graphene deposited with method 15. The single circular white spots are individual gold nanoparticles. A horizontal line scan of 3 pixels wide over the centre of the encircled gold nanoparticle is shown in (b). The FWHM of the line scan is* $12.0 \pm 0.2\,\mathrm{nm}$.

The difference with method 15 is that with method 16 we measured the volume of the drop of gold nanoparticles solution instead of estimated it. Method 16 is depositing 16 µL gold nanoparticles solution with a pipette on graphene on a TEM grid and allowing it to evaporate in the fume hood under atmospheric conditions.

Figure 3.11 shows the deviating structures on the sample made using method 16 that are not observed in the sample made using method 15. Several squares of the TEM grid have regions with increased concentration of gold nanoparticles, see figures 3.11(a) and 3.11(b). We observe several lines of gold nanoparticles on multiple squares of the TEM grid and on the edge of the TEM grid we observe a big blob of gold where a large number of gold nanoparticles have aggregated during the evaporation of the drop of gold nanoparticles solution.

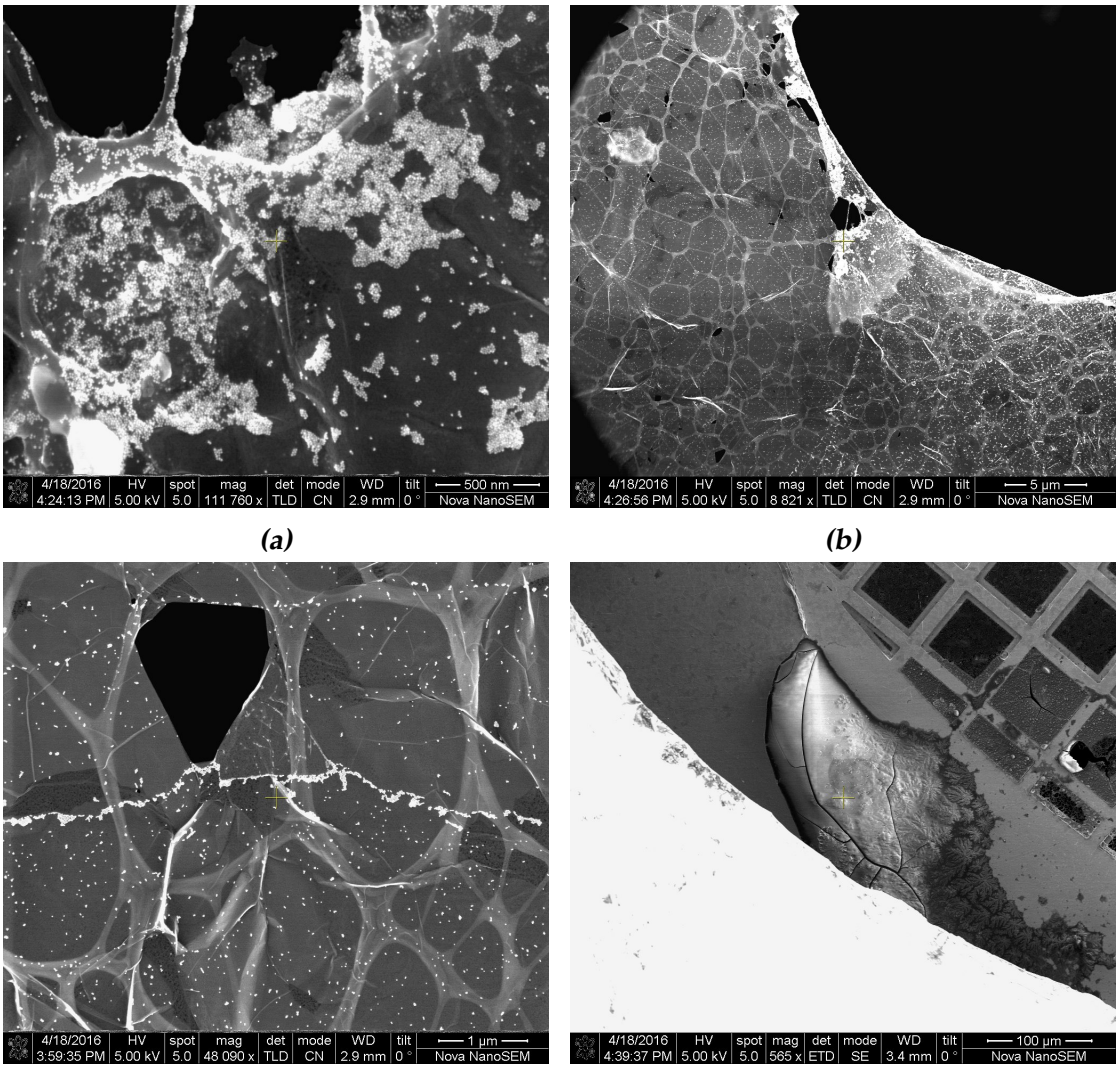

(a) ***(b)***

(c) ***(d)***

Figure 3.11: *(a) High, (b) medium, (c) medium and (d) low magnification SEM images of graphene on a TEM grid after a drop of* 16 µL *gold nanoparticles solution was deposited on it and allowed to evaporate (method 16). (a) shows a region of graphene with a higher concentration and bigger clusters of gold nanoparticles than the rest of the sample, compare with figure 3.9(a). (b) is zoomed out from (a) and has a region with normal concentration of gold nanoparticles on the left and a region of high concentration on the right and at the edges of the big hole in the graphene in the top right. (c) shows a clear linear structure underneath the hole in the graphene and a weaker linear structure above the hole that were not observed using method 15. (d) shows a very large blob of gold on the edge of the TEM grid.*

We try to decrease the time it takes the drops of gold nanoparticles solution deposited on the graphene on a TEM grid to evaporate by putting the TEM grid with the drop in vacuum. Using vacuum to speed up the evaporation is not a suitable method, because of the occurrence of the coffee ring effect, see figure 3.12.

Using method 17 we observe gold nanoparticles rings on the scale of a square of the TEM grid, see figure 3.12(a), and quite a number of clusters of gold nanoparticles including several in one square of a TEM grid with a diameter of roughly 1 µm, see figure 3.12(b).

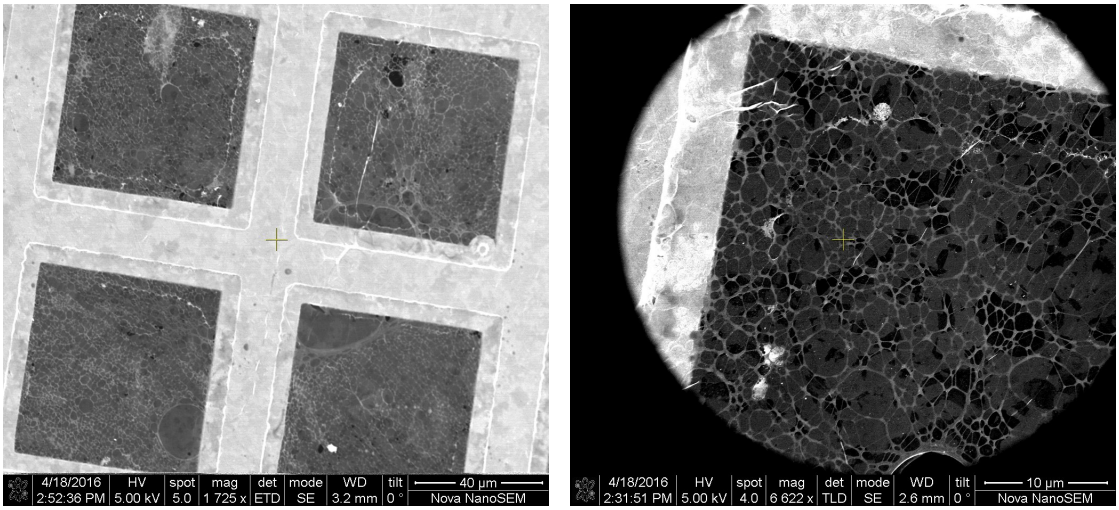

(a) ***(b)***

Figure 3.12: *(a) Low and (b) medium magnification SEM images of graphene on a TEM grid after a drop of* 16 µL *gold nanoparticles solution was deposited on it and evaporated in vacuum (method 17). (a) shows gold nanoparticles rings in multiple squares of the TEM grid. (b) shows graphene with gold nanoparticles and several big clusters of gold nanoparticles with a diameter of roughly* 1 µm *in one square of the TEM grid.*

Method 17 is the same as method 16 except the sample was put in vacuum to evaporate the drop of gold nanoparticles solution faster. Method 17 also results in a lower concentration of gold nanoparticles on the graphene than using method 16.

Version of 18-08-2016– Created August 18, 2016 - 11:48

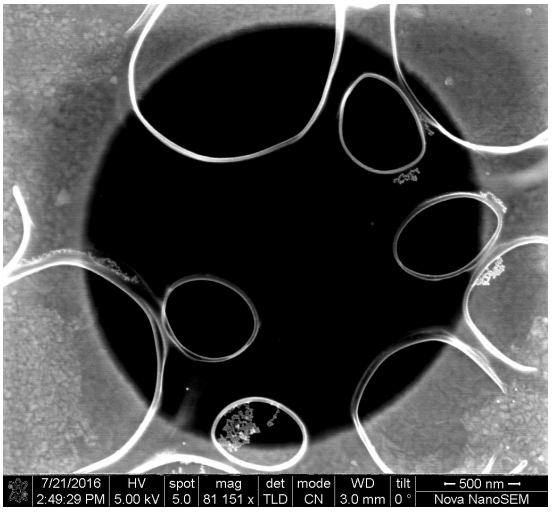

Figure 3.13: *SEM image of gold nanoparticles on graphene on a silicon nitride grid deposited with method 18. The hole in the grid is covered with graphene and largely also with the lacey carbon, which is transparent in this image. We see several groups of gold nanoparticles of which the one in the bottom sits on freestanding graphene whereas the others sit on either lacey carbon or on graphene on top of the grid.*

After transferring graphene to a silicon nitride grid as described in subsubsection 2.2, we deposit 6 ± 2 µL cleaned gold nanoparticles solution with a pipette on graphene on a silicon nitride grid and allow it to evaporate in the fume hood under atmospheric conditions, see figure 3.13. This is method 18.

We see several groups of gold nanoparticles of which the one in the bottom sits on freestanding graphene whereas the others sit on either lacey carbon or on graphene on top of the grid. We do not suffer from the coffee ring effect using method 18.

Figure 3.13 was taken after the sample was imaged with eV-TEM, see figure 3.27(a). This shows we can image gold nanoparticles on graphene with eV-TEM without damaging the sample.

3.2 Ferritin on graphene

We want to deposit ferritin on graphene in such a way that we can image it with LEEM and eV-TEM. In order to determine the best method to deposit ferritin on graphene we use the following six methods to deposit ferritin on graphene on a TEM grid:

Table 3.2: *Ferritin deposition methods. 'Drops' denotes how many drops of ferritin solution we put on the graphene. 'Volume' denotes the volume of the drop we put on the graphene. 'Dilution factor' denotes how much diluted the used ferritin solution is from the starting solution. 'Tissue or evaporation' denotes whether we put the drop of ferritin solution on a TEM grid with graphene with a pipette, suck it up with a paper tissue after* 30 s *and carefully blow it dry with nitrogen gas or put the drop of ferritin solution on a TEM grid with graphene with a pipette and let the drop evaporate at normal pressure and temperature.*

Method	Drops	Volume	Dilution factor	Tissue or evaporation
1	1	16 µL	1000	Tissue[a]
2	3	16 µL	1000	Tissue
3	1	16 µL	10^5	Tissue
4	3	16 µL	10^5	Tissue
5	1	16 µL	10^5	Evaporation
6	1	16 µL	7.6×10^6	Evaporation

[a] 35 s was waited instead of 30 s

From now on we refer to the methods in table 3.2 when using method numbers.

Sucking up a drop on graphene with a tissue removes part of the graphene from the TEM grid. We regularly notice a small black speck on the tissues after sucking up a drop from the graphene. We see more holes in the graphene after using methods 2 and 4 than after depositing ferritin with methods 1, 3, 5 and 6.

We look at all six samples of graphene on a TEM grid with the different ferritin deposition methods with the optical microscope, but only four of the methods are investigated into more detail. We look at samples prepared with methods 2, 3 and 6 with the SEM and at the sample prepared with method 1 with the AFM.

We do not observe the coffee ring effect after having deposited ferritin on graphene on a TEM grid, neither on the level of the entire TEM grid nor on the

level of squares of the TEM grid nor on the level within a square of the TEM grid.

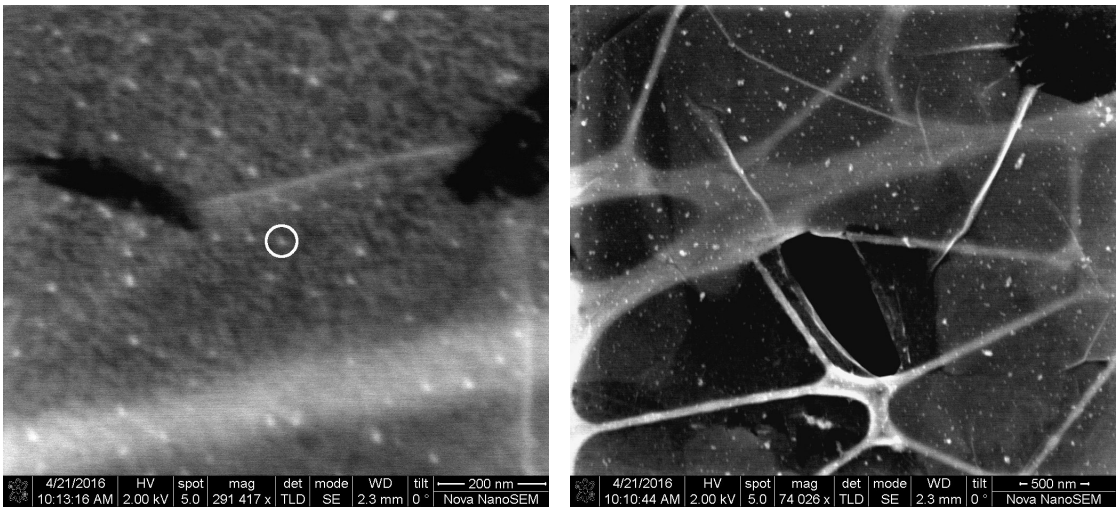

(a) ***(b)***

Figure 3.14: *SEM images at very high (a) and high (b) magnification of ferritin deposited on graphene on a TEM grid using method 2 (putting* 16 µL *1000 times diluted ferritin solution on graphene, sucking it dry with a tissue after* 30 s*, carefully blowing it dry with nitrogen gas and repeating this twice). This is the highest dose of ferritin of the tested deposition methods. In (a) a lot of small white spots and some slightly larger white spots can be observed. The white spots are most likely single proteins or clusters of proteins In (b) we see plenty of small white spots, but also a lot of larger clusters of proteins. The FWHM of the line scans of the encircled spot in (a) is* 15.5 ± 0.5 nm *horizontally and* 16.2 ± 0.5 nm *vertically.*

Method 2 is the highest dose of ferritin we deposit on graphene and figure 3.14 shows what this looks like. At high magnification a lot of small white spots and some larger white spots can be seen. The white spots are most likely single proteins or clusters of proteins since they are not observed in samples without ferritin deposited on them, see figure 3.2 for comparison. These images are typical for what the ferritin on graphene looks like and no very large clusters of ferritin are observed.

We measure the size of the encircled white spot in figure 3.14(a) on the graphene with a line scan of 3 pixels wide. Figure 3.15 shows that the FWHM of the line scans of the ferritin molecule 15.5 ± 0.5 nm horizontally and 16.2 ± 0.5 nm vertically. The line scan is 3 pixels wide to minimise the effects of noise.

We are unable to make a sharp image of individual proteins with the SEM at higher magnification than in figure 3.14(a), partly due to the fact that one cannot

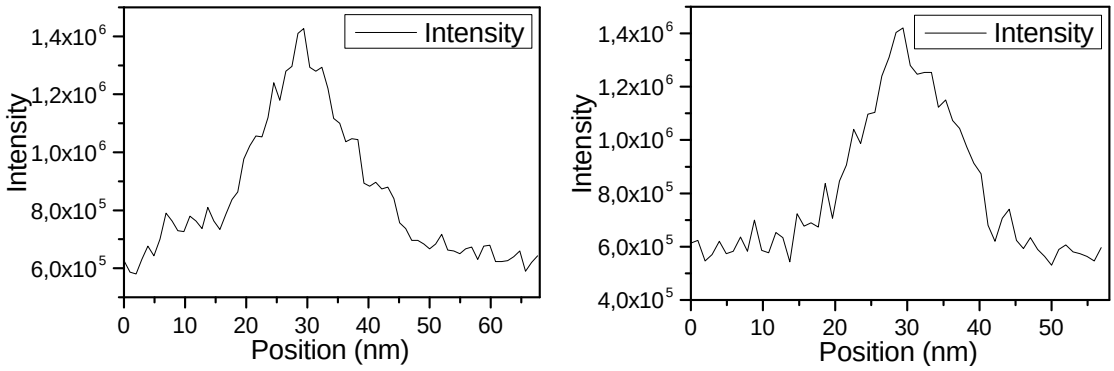

(a) ***(b)***

Figure 3.15: *Line scans of 3 pixels wide in the (a) horizontal and (b) vertical direction of the encircled white spot in figure 3.14(a). The FWHM of the line scans is* 15.5 ± 0.5 nm *horizontally and* 16.2 ± 0.5 nm *vertically.*

look at the same part of the graphene at very high magnification for more than a couple of minutes.

Using method 3 to deposit ferritin on graphene on a TEM grid results in hardly any proteins on the graphene as can be seen in figure 3.16. Method 3 uses a 100 times more diluted ferritin solution and only one drop was put on the TEM grid, while three were used using method 2. The white spots in figure 3.16(a) are one of the few proteins we find on freestanding graphene on the entire TEM grid. We see with the SEM several squares of the TEM grid without any proteins.

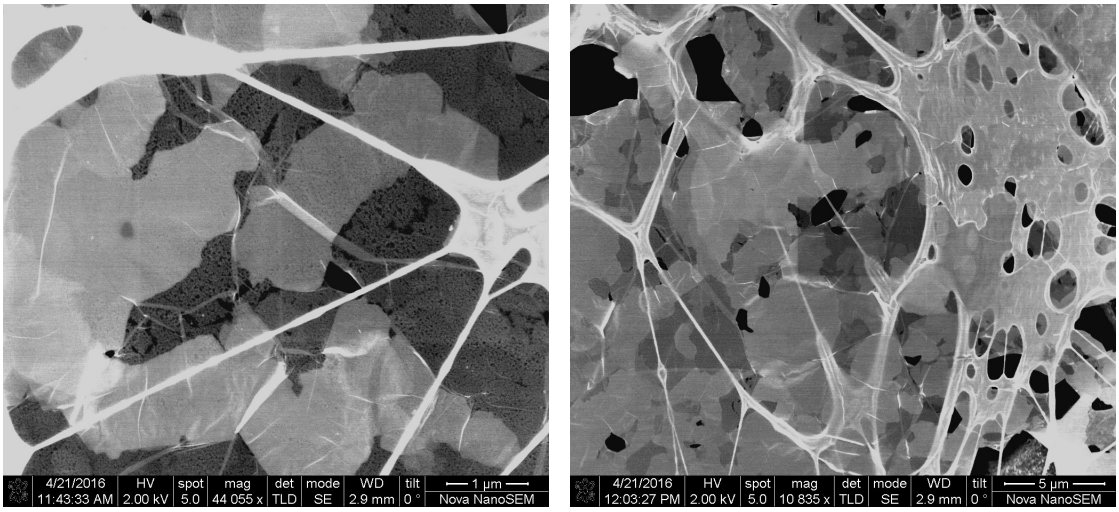

(a) ***(b)***

Figure 3.16: *SEM images at high (a) and medium (b) magnification of ferritin deposited on graphene on a TEM grid with method 3 (putting* 16 µL *10^5 times diluted ferritin solution on graphene, sucking it dry with a tissue after* 30 s *and carefully blowing it dry with nitrogen gas). In comparison to figure 3.14 100 times more diluted ferritin solution is used and only one drop is put on the TEM grid. In (a) we see a couple of small white spots on quite a large area, while in (b) we find no proteins in another, even larger area.*

Using method 6 to deposit ferritin on graphene on a TEM grid results in hardly any proteins on the graphene. In comparison to figure 3.16 a 76 times more diluted ferritin solution is used and the drop is allowed to evaporate instead of being sucked up after 30 s. This is the concentration of ferritin we calculated in subsection 2.1.2 to be needed for a good dispersion of ferritin molecules on the graphene. We find very few proteins on freestanding graphene on the TEM grid and several squares of the TEM grid do not have proteins at all.

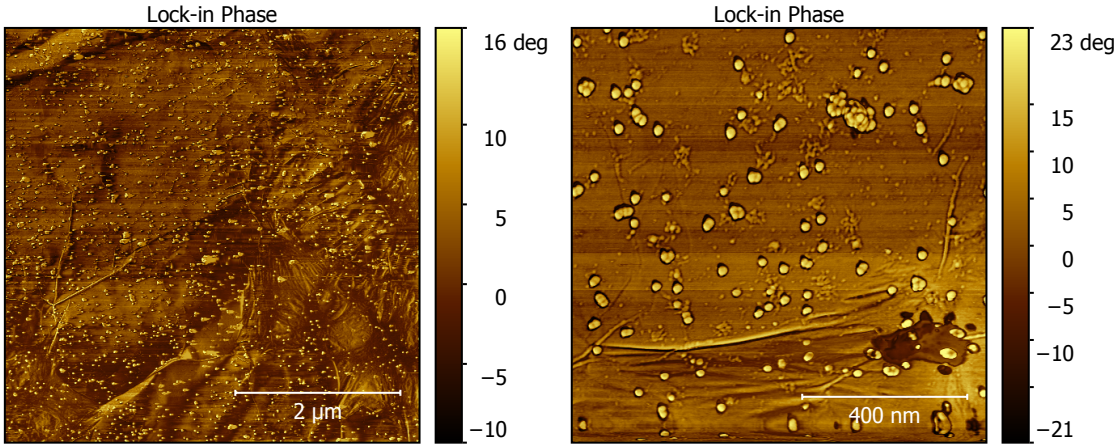

(a) ***(b)***

Figure 3.17: *512 x 512 pixels AFM images of graphene on a TEM grid with ferritin deposited on it with method 1 (putting* 16 µL *1000 times diluted ferritin solution on graphene, sucking it dry after* 30 s *with a tissue and carefully blowing it dry with nitrogen gas). (a) shows the dispersion of ferritin over a* 5 µm × 5 µm *area of graphene in the middle of a square of the TEM grid. (b) shows the dispersion of ferritin over a* 1 µm × 1 µm *area of graphene in the middle of a square of the TEM grid. The approximately round single particles and clusters of them are most likely ferritin molecules. In 3.17(b) we also see contamination on the graphene.*

Using method 1 to deposit ferritin on graphene on a TEM grid results in a good amount of particles, which most likely are proteins, on the graphene with mostly individual proteins, see the AFM images of figure 3.17 for the spread of the proteins on the graphene. In comparison to figure 3.16 a 100 times higher concentration of ferritin solution is used. Individual proteins are clearly visible in figure 3.17(b), but one can better see how the ferritin looks like on the graphene in the smaller area AFM image of figure 3.18.

The diameter of the ferritin molecules in the AFM image of figure 3.18 is 33 nm, which is the average of the diameters of the single molecules from top right to bottom left (35 nm, 33 nm, 29 nm and 34 nm, which are the averages of the lengths of the vertical and horizontal lines in figure 3.18(a)). In figures 3.18(a), 3.18(b) and 3.18(d) we see inner rings in the particles.

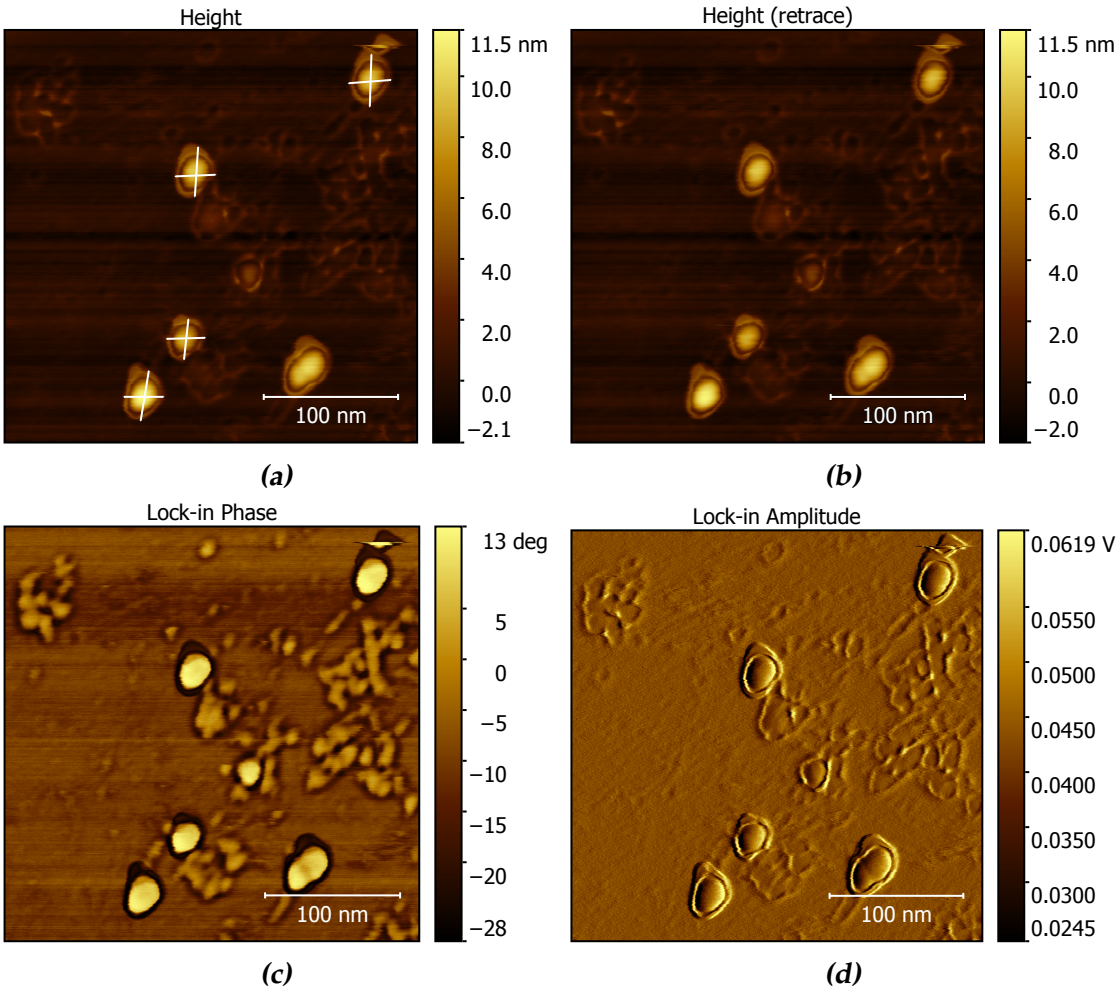

Figure 3.18: *1024 x 1024 pixels AFM images of a* 306 nm × 306 nm *area of graphene on a TEM grid with ferritin deposited on it with method 1 (putting* 16 µL *1000 times diluted ferritin solution on graphene, sucking it dry with a tissue after* 30 s *and carefully blowing it dry with nitrogen gas). (a) and (b) are height profiles showing (a) trace and (b) retrace. The height images are levelled by a flatten base levelling algorithm. (a) The diameter of the four single particles is on average* 33 nm. *(c) shows the lock-in phase and (d) the lock-in amplitude caused by the interaction between the tip and the sample.*

3.3 Flatter graphene on a silicon nitride grid

Performing measurements on graphene on a TEM grid with eV-TEM is tedious, because it costs a lot of time to correct sample tilt. Tilting the sample results in a lateral movement, but the local sample tilt is different after a lateral movement, because a large area of freestanding graphene is very wrinkled.

In order to make the graphene flatter, less wrinkled and easier to handle with eV-TEM, we transfer graphene from a TEM grid to a silicon nitride grid coated with a conducting layer. The graphene coverage of the TEM grids is typically 60 % to 90 %. In this section we show the results of different transfer processes and a comparison of the flatness of graphene on a TEM grid and on a silicon nitride grid.

Graphene on a TEM grid

We observed that the TEM grid with graphene is not flat, see figure 3.19. The only difference between figures 3.19(a) and 3.19(b) is the height at which the optical microscope is focused. The copper bars of the TEM grid are clearly not at the same height as the freestanding graphene.

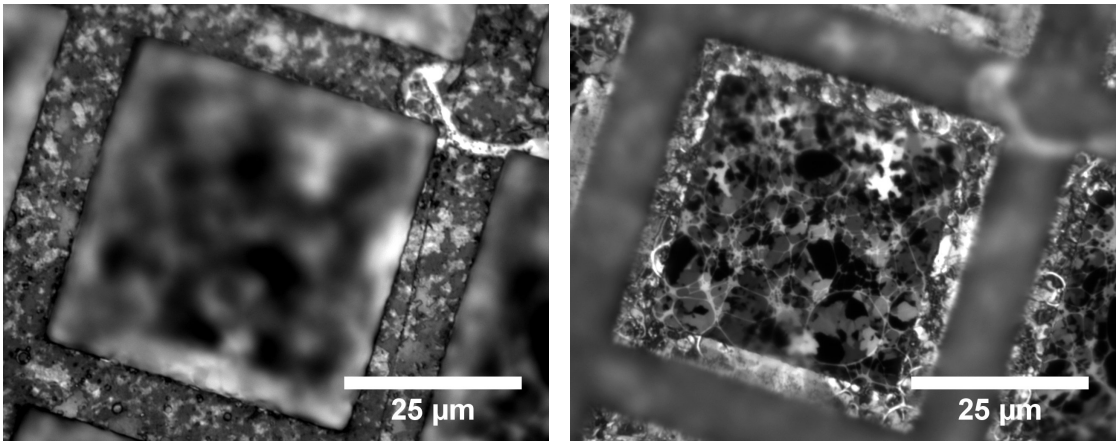

(a) ***(b)***

Figure 3.19: *Optical microscope images of graphene on a TEM grid. The only difference between (a) and (b) is the height at which the optical microscope is focused. This clearly demonstrates a height difference between the bars of the TEM grid and the freestanding graphene.*

We tried to measure the flatness of freestanding graphene on a TEM grid using the profilometer and the AFM. Measuring the flatness of freestanding graphene

Version of 18-08-2016– Created August 18, 2016 - 11:48

using the profilometer does not work, because the tip moves horizontally while in contact with the graphene and destroys it.

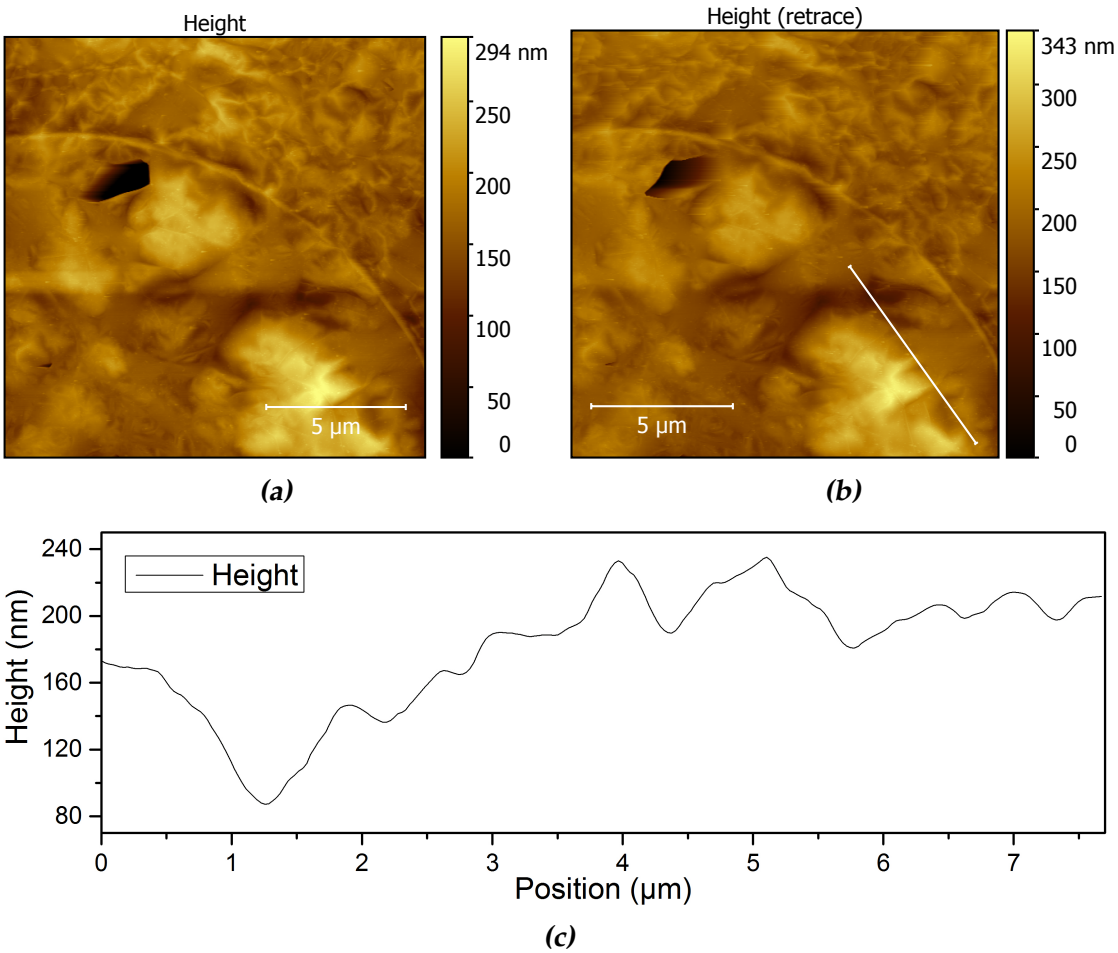

Figure 3.20: *512 x 512 pixels AFM images of the (a) height (trace) and (b) height (retrace) of a* 15 µm × 15 µm *area of graphene on a TEM grid. These images were levelled by mean plane subtraction and the minimum data values were shifted to 0. This process was done excluding the hole in the graphene. (c) Height profile of the line in (b) from the middle to the bottom right.*

We measured a maximum height difference of 319 nm (the average of 294.4 nm and 343.7 nm) in 15 µm × 15 µm freestanding graphene on a TEM grid, see figure 3.20. These AFM images show the trace (figure 3.20(a)) and retrace (figure 3.20(b)) of the height of a 15 µm × 15 µm part of graphene in the centre of a square of a TEM grid. The images were levelled by mean plane subtraction and the minimum data values were shifted to 0. This process was done excluding the hole in the graphene. The height profile of the line in figure 3.20(b) can be

seen in figure 3.20(c) and shows that the freestanding graphene on a TEM grid is not flat anywhere.

Graphene transfer

Table 3.3 summarizes the various graphene transfer methods and whether they were successful or not. From now on we refer to the methods in table 3.3 when using method numbers.

Table 3.3: *Graphene transfer methods. 'Coating' denotes the conducting layer that was sputtered on the silicon nitride grid. 'Drying agent' denotes the drying agent used to make the graphene stick to the silicon nitride grid. 'Graphene transfer' denotes whether the graphene transfer was successful or not.*

Method	Coating	Drying agent	Graphene transfer
1	Cr	Isopropanol	Minimal
2	CrW	Isopropanol	Yes
3	Cr	Chloroform	
4	CrW	Chloroform	
5	Ti	Isopropanol	Yes

When placing the TEM grid with graphene on the silicon nitride grid, one can place the TEM grid with the graphene facing down or with the graphene facing up on the silicon nitride grid. We found that we need to place the TEM grid with graphene facing down for the graphene transfer to be successful. All methods in table 3.3 are with the graphene facing down.

Using method 1 we transferred only a small amount of graphene from a TEM grid with graphene to a silicon nitride grid. Method 1 is putting a TEM grid with graphene on a chromium coated silicon nitride grid and isopropanol in between.

Version of 18-08-2016– Created August 18, 2016 - 11:48

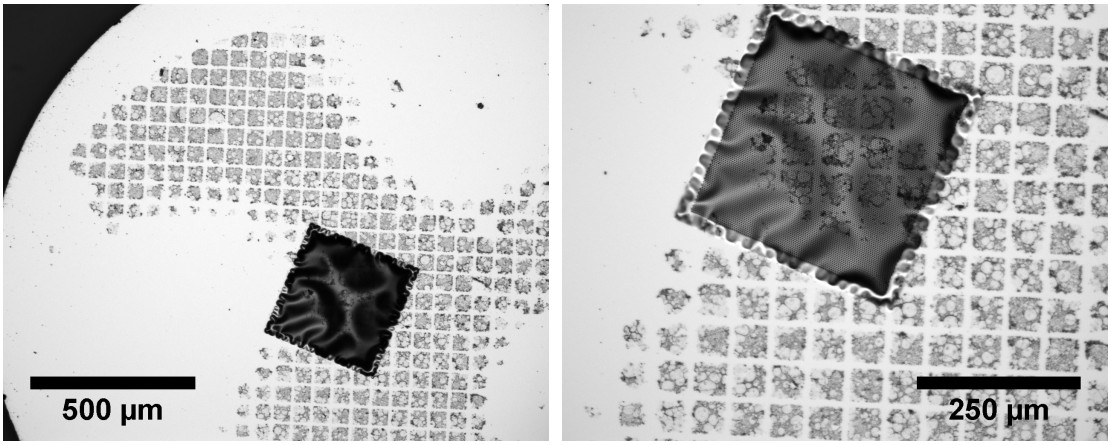

(a) *(b)*

Figure 3.21: *Optical microscope images of graphene on a silicon nitride grid coated with chromium and tungsten (method 2). (a) Basically all graphene was transferred from the TEM grid to the silicon nitride grid. We see a lot of squares of lacey carbon, which have graphene underneath. The uncovered parts of the silicon nitride grid are due to the fact that the TEM grid had a coverage of approximately 60%. (b) The graphene on the* 200 nm *thick silicon nitride square covers a large part of the square.*

Using method 2 we transferred graphene from a TEM grid with graphene to a silicon nitride grid, see figure 3.21. Basically all graphene was transferred from the TEM grid to the silicon nitride grid. The uncovered parts of the silicon nitride grid have no graphene, because that part of the TEM grid had no graphene. In figure 3.21(b) we see that plenty of holes in the silicon nitride are covered with graphene, but this is not always as good as shown here, because the graphene coverage of the TEM grids is usually 60 % to 90 %. Method 2 is putting a TEM grid with graphene on a silicon nitride grid coated with chromium and tungsten and isopropanol in between.

The graphene transfer process was unsuccessful using chloroform as a drying agent, slowly heating it to ≈200 °C and keeping it at ≈200 °C for 5 minutes (methods 3 and 4). This is true regardless of the sputtered conducting layer(s).

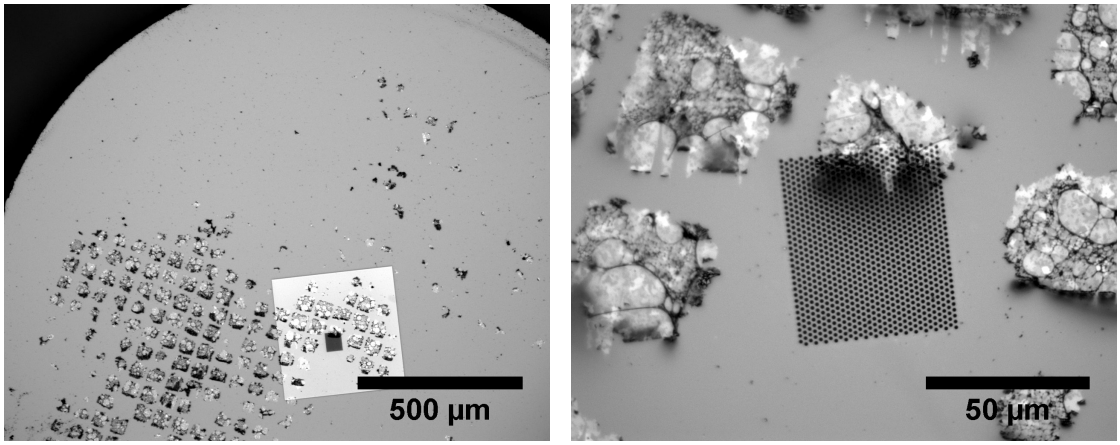

(a) *(b)*

Figure 3.22: *(a) Low and (b) high magnification optical microscope images of graphene on a silicon nitride grid coated with titanium (method 5). (a) Only roughly a third of the silicon nitride grid is covered with graphene. The visible squares are lacey carbon, which have graphene underneath. (b) is zoomed in at the area with holes in the centre of the square of* 200 nm *thick silicon nitride. With such a small area of holes in the silicon nitride one has to be lucky to have graphene over the holes, which is mostly not the case here.*

Using method 5 we transferred graphene from a TEM grid with graphene to a silicon nitride grid, but only roughly a third of the silicon nitride grid was covered with graphene, see figure 3.22(a). The TEM grid with graphene was almost fully covered with graphene. The square of only silicon nitride was partially covered with graphene and the small area of holes in the silicon nitride is hardly covered with graphene, see figure 3.22(b). Method 5 is putting a TEM grid with graphene on a titanium coated silicon nitride grid and isopropanol in between.

Notice the difference in the size of the area with holes between figures 3.21 and 3.22. The entire square of only 200 nm thick silicon nitride should have holes in order to increase the chance of finding a good hole covered with graphene for measurement with LEEM and eV-TEM.

Graphene on a silicon nitride grid

The goal of the graphene transfer process is to make flatter, less wrinkled graphene for easier eV-TEM measurements. In order to accomplish this we transferred graphene to a silicon nitride grid with holes in the entire square of only 200 nm thick silicon nitride.

A qualitative measurement of the flatness of graphene on a silicon nitride grid is that we observed that aligning and imaging graphene on such a grid with LEEM and eV-TEM is much easier and faster than graphene on a TEM grid.

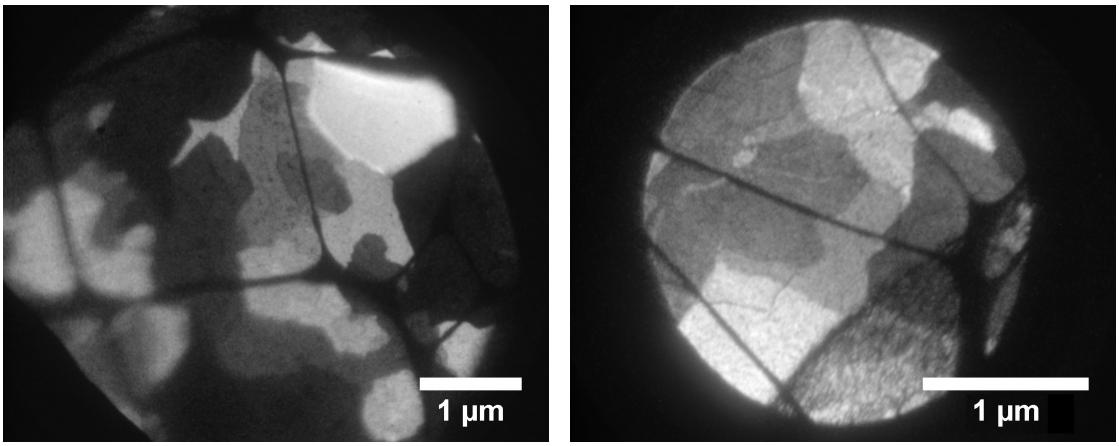

(a) ***(b)***

Figure 3.23: *eV-TEM images of graphene on (a) a TEM grid and (b) a silicon nitride grid. Different grey levels correspond to different graphene layer thicknesses. (a) Part of the graphene is in focus, while another part is not, showing the sample is not flat. The electron energy is* 2.1 eV*. (b) The entire sample is equally in focus, meaning the sample is flat. The electron energy is* 5.1 eV*.*

We observe that only a small area of graphene is in focus at a given time doing eV-TEM on graphene on a TEM grid, while a much larger area of graphene is in focus simultaneously doing eV-TEM on graphene on a silicon nitride grid, see figure 3.23. This shows the graphene is flatter on a silicon nitride grid than on a TEM grid.

If one wants a quantitative measurement of the flatness of graphene on a silicon nitride grid, one can measure this with the AFM.

3.4 Resolution determination

In this section we show the results of our efforts to obtain the best resolution of eV-TEM and we determine what that is.

The imaging system is separate from eV-TEM so we can align the imaging system using LEEM. We aligned the imaging system with PEEM and LEEM using silicon and $SrTiO_3$ (STO) samples, which is much easier than using graphene because graphene does not give a clear diffraction pattern. After aligning the imaging system the sample can be changed and graphene can be imaged with eV-TEM without changing anything to the imaging system.

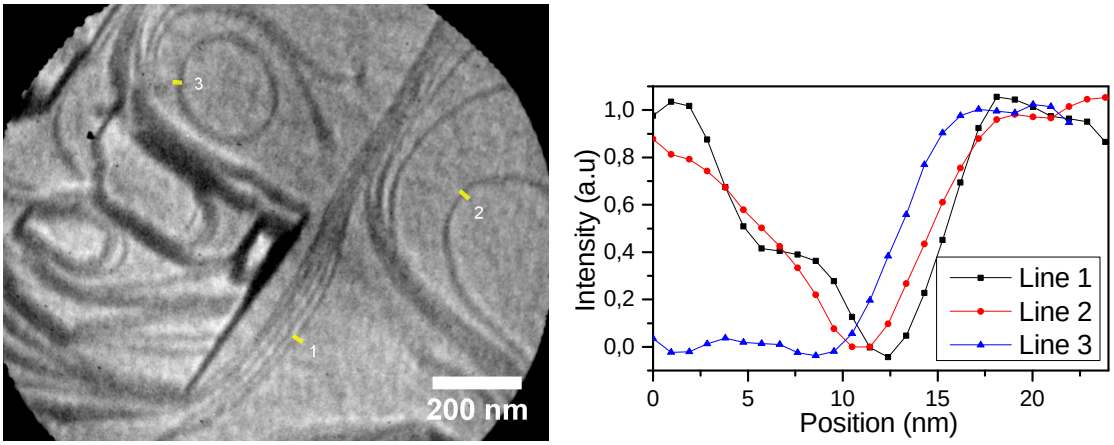

(a) ***(b)***

Figure 3.24: *(a) LEEM image without aberration correction of STO on silicon after alignment with an electron energy of* 18.7 eV. *The spatial resolution is* 3 nm, *which is the average of the three 10 pixels wide line scans. (b) The line scans of the three lines in (a) are 10 pixels wide and normalised to the average of the lower and upper level. The resolutions are* 2.5 nm *(line 1),* 3.6 nm *(line 2) and* 3.1 nm *(line 3).*

We performed several alignment iterations of the imaging system. Directly after the last alignment iteration we made a LEEM image without aberration correction. The spatial resolution of figure 3.24(a) is 3 nm, the average of the resolutions of the 10 pixels wide line scans 1 (2.5 nm), 2 (3.6 nm) and 3 (3.1 nm). The spatial resolution is determined in the same way as in Tromp et al. (2013) [2]. The line scans are 10 pixels wide to minimise the effects of noise. This is the best resolution we obtained without aberration correction. The used substrate was STO on silicon and the lines in the STO are probably step edges.

Version of 18-08-2016– Created August 18, 2016 - 11:48

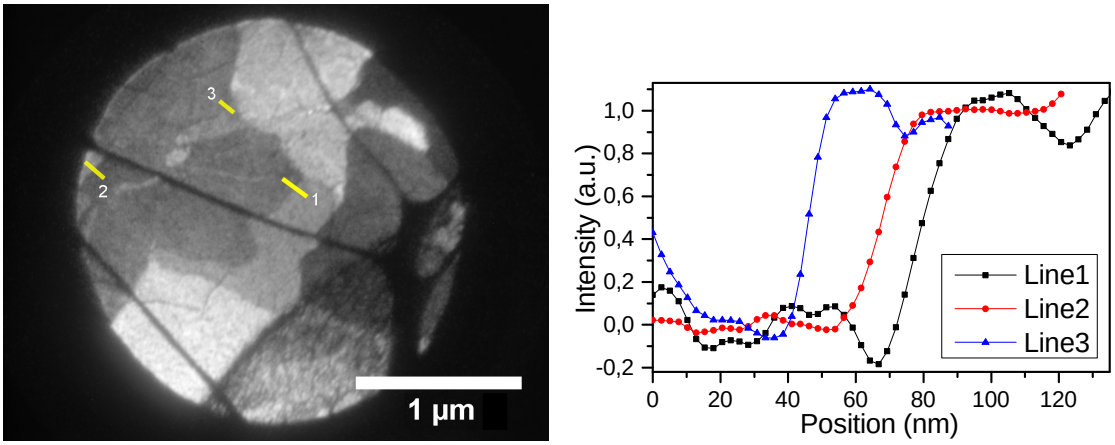

(a) ***(b)***

Figure 3.25: *(a) eV-TEM image of graphene on a silicon nitride grid with the best resolution we obtained with eV-TEM with an electron energy of* 5.1 eV*. Different grey levels correspond to different graphene layer thicknesses. The spatial resolution is* 10 nm*, which is the average of the three 10 pixels wide line scans. (b) The line scans of the three lines in (a) are 10 pixels wide and normalised to the average of the lower and upper level. The resolutions are* 10.4 nm *(line 1),* 9.5 nm *(line 2) and* 9.6 nm *(line 3).*

After alignment of the imaging system we put a silicon nitride grid with graphene in the LEEM and made an image of the best resolution of eV-TEM on graphene, see figure 3.25. Different grey levels correspond to different graphene layer thicknesses.

The spatial resolution of figure 3.25(a) is 10 nm, the average of the resolutions of the 10 pixels wide line scans 1 (10.4 nm), 2 (9.5 nm) and 3 (9.6 nm). The spatial resolution is determined in the same way as in Tromp et al. (2013) [2]. The line scans are 10 pixels wide to minimise the effects of noise.

3.5 Imaging gold nanoparticles with eV-TEM

We want to be able to image gold nanoparticles on graphene with eV-TEM.

The first time we looked at gold nanoparticles on graphene we did not have transmission through the graphene due to contaminants on the graphene from the gold nanoparticles solution, see figure 3.26. The bright areas in figure 3.26 are due to signal through holes in the graphene so eV-TEM was working. The sample we looked at was graphene on a TEM grid with gold nanoparticles deposited on it using method 15 of table 3.1.

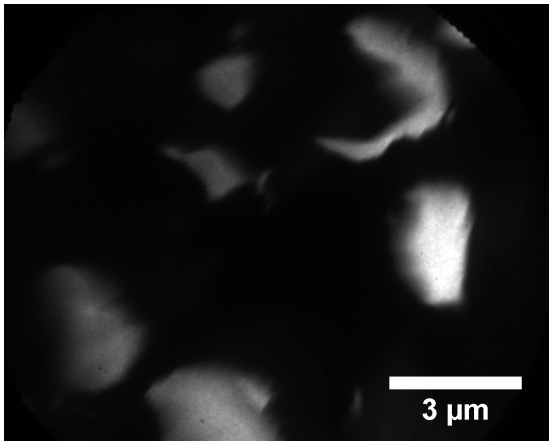

Figure 3.26: *eV-TEM image of graphene on a TEM grid with gold nanoparticles deposited on it with an electron energy of* 2.1 eV*. We were unable to get transmission through the graphene due to contaminants on the graphene from the gold nanoparticles solution.*

After our initial attempt to image gold nanoparticles on graphene with eV-TEM, we cleaned the gold nanoparticles solution as described in subsubsection 2.1.1.

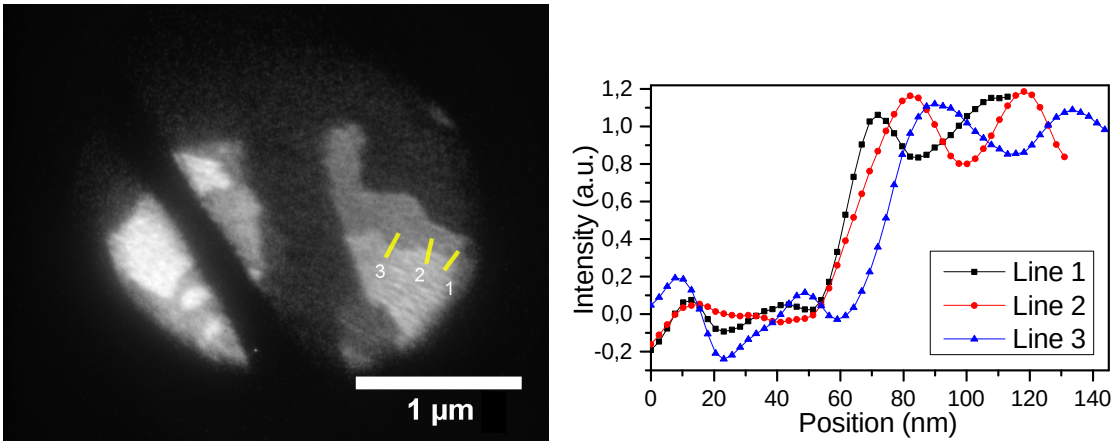

(a) ***(b)***

Figure 3.27: *(a) eV-TEM image of graphene on a silicon nitride grid with gold nanoparticles deposited on it, but no gold nanoparticles can be observed. The electron energy is* 2.7 eV*. Different grey levels correspond to different graphene layer thicknesses. The spatial resolution is* 10 nm*, which is the average of the three 10 pixels wide line scans. (b) The line scans of the three lines in (a) are 10 pixels wide and normalised to the average of the lower and upper level. The resolutions are* 8.3 nm *(line 1),* 12.5 nm *(line 2) and* 10.1 nm *(line 3).*

With cleaned gold nanoparticles solution deposited on graphene on a silicon nitride grid using method 18 of table 3.1 we did have transmission through the graphene with eV-TEM, see figure 3.27. Unfortunately we were unable to observe individual or groups of gold nanoparticles. Figure 3.27(a) is not very good because the eV-TEM cathode was broken at the time. This made properly aligning the eV-TEM illumination impossible. After this eV-TEM measurement, we confirmed with the SEM that we have gold nanoparticles on this sample, see figure 3.13.

The spatial resolution of figure 3.27 is 10 nm, the average of the resolutions of the 10 pixels wide line scans 1 (8.3 nm), 2 (12.5 nm) and 3 (10.1 nm). The spatial resolution is determined in the same way as in Tromp et al. (2013) [2]. The line scans are 10 pixels wide to minimise the effects of noise.

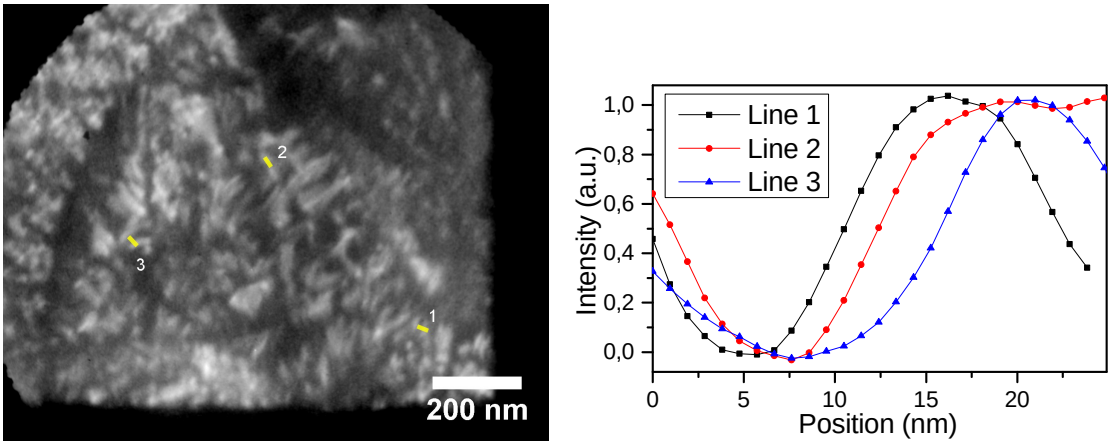

(a) ***(b)***

Figure 3.28: *(a) LEEM image of graphene on a silicon nitride grid with an electron energy of* 2.2 eV*. This is the best resolution we obtained with LEEM of graphene on a silicon nitride grid. On the left a section of the circle that is the edge of the hole in the grid can be seen. So everything except the leftmost graphene is freestanding graphene. The spatial resolution is* 4 nm*, which is the average of the three 10 pixels wide line scans. (b) The line scans of the three lines in (a) are 10 pixels wide and normalised to the average of the lower and upper level. The resolutions are* 3.9 nm *(line 1),* 4.0 nm *(line 2) and* 4.4 nm *(line 3).*

The spatial resolution of figure 3.28(a) is 4 nm, the average of the resolutions of the 10 pixels wide line scans 1 (3.9 nm), 2 (4.0 nm) and 3 (4.4 nm). The spatial resolution is determined in the same way as in Tromp et al. (2013) [2]. The line scans are 10 pixels wide to minimise the effects of noise. This is the best resolution we obtained with LEEM on graphene on a silicon nitride grid. This proves that it is possible to obtain a resolution on graphene on a silicon nitride grid that is good enough to see individual gold nanoparticles.

We know that eV-TEM has a resolution that is good enough to see groups of gold nanoparticles, but maybe not individual ones and we know that we have transmission through the graphene after we deposited cleaned gold nanoparticles solution on it so we should be able to image gold nanoparticles with eV-TEM.

Chapter 4

Discussion

4.1 Gold nanoparticles deposition

In this section we discuss the results of the deposition of gold nanoparticles on graphene and silicon. We start by discussing the occurrence and effect of the coffee ring effect. The coffee ring effect leads to the aggregation of gold nanoparticles, which makes it impossible to image (part of) the sample with eV-TEM.

We found a method of depositing gold nanoparticles on graphene that creates a sample that we can image with LEEM and eV-TEM. This is method 16 of table 3.1. Part of the sample sometimes has coffee ring structures, but this is not a problem as a large part of the sample is usable. Not holding the grid with graphene exactly horizontal during deposition might cause the coffee ring effect to occur.

In general we can say the coffee ring effect is less on graphene than on silicon and outside influences like evaporation conditions apply on both roughly the same. Problematic coffee ring structures occur on silicon as a result of gold nanoparticles deposition, but the coffee ring effect is not a problem for gold nanoparticles deposition on graphene even if it occurs.

Graphene is a very different material from silicon wafer so applying results from silicon to graphene is not straight forward. Graphene has holes, step edges and lacey carbon strands and freestanding graphene is not as flat as a polished metal surface, all of which probably helps suppressing the coffee ring effect.

The conditions during drop evaporation affect the occurrence of the coffee ring effect. Temperature, pressure, air currents might all be of influence. We determined that letting a drop of gold nanoparticles solution on graphene evaporate in vacuum increases the coffee ring effect. The vacuum is of a maximum pressure in the order of 10 mbar. The gauge of the load lock is linear and thus not precise at all for low pressures.

Next we discuss the effects and necessity of cleaning the gold nanoparticles solution and/or the substrate.

We found in our silicon experiments that a cleaner surface makes the coffee ring effect weaker. We do not know if this is true for graphene as well, but our results indicate this is not relevant.

We should be able to image individual gold nanoparticles with eV-TEM with better resolution as described in section 3.5. Cleaning the gold nanoparticles solution solved the problem of not getting transmission through the graphene with eV-TEM, but we have not been able to image individual gold nanoparticles with eV-TEM yet.

Cleaning the graphene before deposition might give more and better signal through the graphene, but at the moment cleaning graphene before deposition seems unnecessary. Properly cleaning graphene is hard, see e.g. Algara-Siller et al. (2014a) [5].

We cleaned the gold nanoparticles solution by washing it twice. Washing it more than two times might give more and better signal through the graphene, but we believe that this is not necessary. After separating the particles from the solvent by centrifuging the solution, we take almost all solvent up with a pipette and add roughly the same amount of clean solvent. Less than 20 µL of 1 mL remains after taking up the solvent so the amount of contaminants is reduced by at least 98 % after washing assuming the added type 1 water and the new pipette tip used are really clean.

The gold nanoparticles concentration is probably not exactly the same as before the washing, but we do not need a certain exact amount of gold nanoparticles on our graphene so this is not a problem.

Now we discuss the measurement of the size of a white spot in a SEM image, which has the purpose of determining if it is a gold nanoparticle.

The white spots in SEM images look like they are gold nanoparticles, see e.g. figure 3.9(b), but we also zoomed in at a single white spot and measured its size, see figure 3.10.

The Full Width at Half Maximum (FWHM) of the gold nanoparticle we zoomed in at in figure 3.10(a) is 12.0 ± 0.2 nm, while the diameter of the gold nanoparticles should be $\approx$10 nm. We cannot simply say its diameter is indeed 10 nm because the SEM is not an ideal method to measure the size of nanoparticles. The intensity and size of the nanoparticles depend on the brightness and contrast setting of the SEM. A line scan over the centre of a particle is not a step function, but looks like a Gaussian function. We give the FWHM of the line scan as indication of the particle size because this is an established and reproducible procedure to say something about a distribution.

Also not all particles look equally big. In figure 3.10(a) we see three more individual gold nanoparticles and they all look smaller than the encircled particle. They probably are smaller, because the synthesis process does not create particles that are all exactly the same size. Furthermore, the best resolution of this SEM is $\approx$2 nm. For a better size determination one should use a TEM, which has a much better resolution.

Even though we cannot say the particles we see have a diameter of exactly 10 nm, our measurement shows with sufficient accuracy that we do have gold nanoparticles on graphene.

We use a pipette that is calibrated for 20 µL to 200 µL and we deposit drops that are slightly under the calibrated range so their volume is not guaranteed to be what the pipette indicates. We need an amount and dispersion of nanoparticles that we can image so the volume can deviate somewhat in each case without consequences.

For experiments with LEEM and eV-TEM samples should be used that have not been looked at with the SEM. The high energy electrons of the SEM damage the graphene.

We checked only one sample of gold nanoparticles on graphene on a silicon nitride grid with the SEM and that was with a smaller volume of gold nanoparticles solution than our best method, but we did have gold nanoparticles on freestanding graphene. We expect that depositing cleaned gold nanoparticles solution on a silicon nitride grid using method 16 of table 3.1 results in a sample on which we can see groups of gold nanoparticles with LEEM and eV-TEM.

4.2 Ferritin on graphene

In this section we discuss the results of the deposition of ferritin on graphene and the expected feasibility of imaging this with LEEM and eV-TEM.

We found a method of depositing ferritin on graphene that creates a sample that we believe we should be able to image with LEEM and eV-TEM.

However, cleaning the ferritin solution might be needed to successfully image ferritin (or another protein or DNA) on graphene with eV-TEM. We observe some contaminants on graphene with the AFM, see figure 3.18, but we do not know whether it is due to ferritin deposition or it was present before. Our ferritin comes in a 0.15 M NaCl solution, which can be largely removed by dialysis. We dilute the ferritin solution a thousand times so the salt and other contaminants are also diluted already.

Proteins are folded in a certain way and this determines not only their form, but also their activity. Their activity is irrelevant for imaging purposes, but a suitable deposition method is needed if proteins are to be studied with LEEM and eV-TEM in normal working condition. Then the pH of the solution needs to be kept in a suitable interval with a pH buffer for dialysis and dilution.

We do not use a pH buffer because we do not perform extensive measurements on ferritin and only want to see how the ferritin ends up on graphene and if we could image this with LEEM and eV-TEM.

We choose to deposit ferritin on graphene on a TEM grid by putting a drop on the grid, sucking it up with a paper tissue after 30 s and carefully blowing it dry with nitrogen gas. We do not allow the drop to evaporate because this way we do not get all the salt and other contaminants in the solution that do not evaporate on the graphene. Additionally we do not suffer from the coffee ring effect and from damage to the folding of the proteins during evaporation.

An alternative for sucking the drop up with a tissue is rinsing it away with type 1 water, but that has to be done carefully in order not to wash away the TEM grid altogether. TEM grids are quite fragile. This is a viable alternative however for depositing ferritin solution on graphene on a silicon nitride grid.

Using a tissue to suck up the drop of ferritin solution removes part of the graphene from the TEM grid too. However we find that this is not really a problem because we still have a large part of the graphene with ferritin to image when we deposit and suck up only one drop. It is unknown if sucking up a drop damages graphene on a silicon nitride grid. If this turns out to be a problem, one can see if rinsing a drop away with type 1 water does not damage graphene.

Version of 18-08-2016– Created August 18, 2016 - 11:48

Now we discuss the measurement of the size of a white spot in a SEM image and of a particle in an AFM image, which has the purpose of determining if it is a ferritin molecule.

The white spots in SEM images look like they are ferritin molecules. The FWHM of the line scans of the encircled spot in figure 3.14(a) is 15.5 ± 0.5 nm horizontally and 16.2 ± 0.5 nm vertically. The particles in the AFM images really look like they are ferritin molecules. The particles in the AFM image of figure 3.18 have an average diameter of 33 nm, which was crudely measured by averaging the lengths of lines horizontally and vertically over the full size of the particles.

A ferritin molecule in a liquid is roughly a sphere with a diameter of 12 nm consisting of 24 sub-units and it is likely it expands in the lateral dimensions while it is lying on a surface. The observed particles in figures 3.14(a) and 3.18 are not found on the control sample and the SEM and AFM images suggest the size is correct. So we are sure we have indeed ferritin molecules on graphene.

We have only deposited ferritin on graphene on a TEM grid, but we expect to be able to deposit ferritin on graphene on a silicon nitride grid in the same way.

We have a spatial resolution with LEEM and eV-TEM that is good enough to image individual proteins. We expect to be able to image ferritin for an extended period of time with low enough landing energies. LEEM and eV-TEM can destroy proteins though if the electrons have a sufficiently high energy when arriving at the sample.

4.3 Flatter graphene on a silicon nitride grid

In this section we discuss the graphene transfer process and the effect it has on eV-TEM measurements.

We found a method of transferring basically all the graphene from a TEM grid to a silicon nitride grid. The transfer works very well as evidenced by figure 3.21. Using a coating of tungsten on top of chromium and using isopropanol to make the graphene stick to the silicon nitride grid works best.

One should be beware that the graphene coverage of a TEM grid varies significantly and that only the small part of the silicon nitride grid with holes is usable for eV-TEM measurements. This means that we need to look at the TEM grid with graphene before the transfer and sometimes be a littly lucky. This also means that one should use a grid with holes in the entire centre square and not in only a part of the square as our initial samples had.

Imaging graphene on a silicon nitride grid is much faster than on a TEM grid and it also works better. Correcting sample tilt for graphene spanning a large square of a TEM grid takes a long time because the graphene is very wrinkled and tilting the sample results in lateral movement, which in turn changes the local sample tilt. The graphene over a hole in a silicon nitride grid is much flatter, compare figure 3.23(b) to figures 3.19 and 3.20. This means correcting sample tilt on a silicon nitride grid is straightforward.

It also means a larger area of graphene is in focus simultaneously and image quality is higher as well. Qualitatively speaking the transfer process constitutes a great improvement in measuring with eV-TEM. This is as we expected because the holes in a silicon nitride grid are much smaller than in a TEM grid.

We heated graphene on a silicon nitride grid and produced very clean graphene and the coating did not break off in the process. This is important for eV-TEM, but not for gold nanoparticles or ferritin deposited on graphene.

One could use the AFM to measure the flatness of graphene on a silicon nitride grid for a quantitative comparison with a TEM grid, but this is not necessary because the practical difference is huge.

We did measure the flatness of graphene on a TEM grid and we found quite a height difference. The choice of the levelling algorithm influences the height difference with the way we measure it. Hence we are not sure of what the AFM images can tell us exactly, but this is not really a problem because again the practical difference between graphene on a TEM and on a silicon nitride grid is huge.

Version of 18-08-2016– Created August 18, 2016 - 11:48

4.4 Resolution determination

In this section we discuss our efforts to obtain the best resolution with eV-TEM and the results of those efforts.

The best spatial resolution we obtain with eV-TEM on graphene is 10 nm. This is the spatial difference between 20 % and 80 % of the difference between the minimum and maximum intensities of an one-dimensional intensity shift. To minimise the effects of noise we make the line scans 10 pixels wide and average three of them. We measure the resolution the same way Tromp et al. (2013) does [2].

This resolution is obtained with a good alignment, the same with which we obtained a resolution of 3 nm on STO with LEEM. This is even without aberration correction. The lines in the STO in figure 3.24(a) are probably step edges. It does not matter though what it is exactly because any one-dimensional intensity shift can be used to determine the resolution.

The difference between the best resolutions with LEEM and eV-TEM is due to differences in sample and illumination technique. The best resolution we obtained on graphene with LEEM is 4 nm, which is still a lot better than the 10 nm of eV-TEM. This is as we expected for the following two reasons: the energy spread of the eV-TEM electron gun is more than three times higher than that of the LEEM gun, 800 meV vs. 250 meV, and with eV-TEM it is hard to make the electron beam incidence exactly perpendicular to the sample, which causes astigmatism.

For the determination of resolution we use the field of view of the used magnification of the microscope. That corresponds pretty well to the true field of view, but it is not calibrated. Because of this our resolutions might be slightly off, but it does not explain why our resolution of LEEM on STO is better than should be possible without aberration correction. Without aberration correction the best obtainable resolution should be $\approx$4 nm [6].

We aligned the imaging system quite well, but not perfectly. It could be better if the magnification at all image planes were calibrated. Our real-space images look very good, but the diffraction could be made better.

Version of 18-08-2016– Created August 18, 2016 - 11:48

4.5 Imaging gold nanoparticles with eV-TEM

In this section we discuss the imaging of gold nanoparticles on graphene with eV-TEM.

We have successfully imaged graphene with gold nanoparticles deposited on it, but we probably need a better resolution to see individual gold nanoparticles. A resolution of 10 nm or better is needed to see particles with a diameter of 10 nm.

Our current best resolution of 10 nm on graphene with gold nanoparticles on it is at the very edge of what is required to see individual gold nanoparticles. It should however already be good enough to see groups of gold nanoparticles, but we have not been able to see such groups. We confirmed the sample had gold nanoparticles on it with the SEM, see figure 3.13. This sample has a lower dose of gold nanoparticles so we expect to be able to see evidence of groups with a sample prepared with the method that we determined works best.

We expect to see dark circular spots and groups of them on graphene where gold nanoparticles lie because they prevent electron transmission or severely reduce it.

At first we did not have transmission through the graphene after we deposited gold nanoparticles on it. We solved this by cleaning the gold nanoparticles solution. This shows that transmission through graphene is sensitive to contaminants on the graphene. With gold nanoparticles (or ferritin) on it graphene cannot be cleaned by heating it in the microscope so one should be careful with what one puts on the graphene.

If we obtain a sufficient resolution but still cannot see gold nanoparticles, contaminants on the graphene from either exposure to air or the deposition process might affect electron transmission. These effects can be minimised by minimising the exposure to air and cleaning the material to be deposited on the graphene.

Version of 18-08-2016– Created August 18, 2016 - 11:48

Chapter 5

Conclusion

5.1 Conclusions

In this section we discuss the conclusions of our research project. The goals of the project were to determine the spatial resolution of eV-TEM and investigate whether we can image something deposited on graphene with eV-TEM. We also present the conclusion about the new way of measuring with eV-TEM with the graphene transfer.

We aligned the imaging system of ESCHER pretty well and used a sample of graphene on a silicon nitride grid to determine the best spatial resolution of eV-TEM. The best resolution we obtained with eV-TEM on graphene was 10 nm, which was determined in the same way as in Tromp et al. (2013) [2].

The resolution of LEEM we measured on STO of 3 nm without aberration correction proves that we aligned the imaging system pretty well. The resolution of eV-TEM can be made a bit better, but it will not be able to be as good as that of LEEM because of the greater energy spread of the eV-TEM cathode.

We have deposited cleaned gold nanoparticles solution on graphene on a silicon nitride grid and we are able to image this with eV-TEM, but we have not observed individual gold nanoparticles yet. We know from SEM images we have groups of gold nanoparticles on freestanding graphene and we should be able to see these. We find that the best method of depositing gold nanoparticles on graphene is to put about 16 µL cleaned gold nanoparticles solution with a pipette on the grid with graphene and let it evaporate.

We deposited ferritin on graphene and we think we should be able to image ferritin with LEEM and eV-TEM. We might need to clean the ferritin solution in order to do so though. We find that the best method of ferritin deposition is to put about 16 µL of 1000 times diluted ferritin solution on the grid with graphene, wait for 30 s and suck the drop up with a paper tissue.

Transferring graphene from a TEM grid to a silicon nitride grid makes the graphene much flatter, less wrinkled and therefore much easier and faster to image with eV-TEM. It also improves image quality. The best way to transfer graphene is to coat the silicon nitride grid on both sides with chromium and tungsten and to use isopropanol to make the graphene of the TEM grid stick to the tungsten after the isopropanol evaporates.

Version of 18-08-2016– Created August 18, 2016 - 11:48

5.2 Outlook

In this section we give an outlook to possible continuations of our research. This includes improving the spatial resolution of eV-TEM by both software and hardware improvements and further studying nanoparticles deposited on graphene with low energy electrons.

A better alignment of the imaging system can give a better spatial resolution of eV-TEM, but the largest improvement will be the replacement of the eV-TEM cathode with a better one. The main way to improve the alignment and thus the resolution of eV-TEM in the current set-up is calibrating the magnification at all image planes in the imaging system.

One can continue to image graphene on a silicon nitride grid with cleaned gold nanoparticles solution deposited on it with eV-TEM. We expect to be able to see groups of gold nanoparticles with the current resolution and individual gold nanoparticles with better resolution.

If seeing gold nanoparticles turns out not to be possible with the current samples, one can try to clean the gold nanoparticles solution even more. If that does not help, AFM imaging of graphene before and after gold nanoparticles solution deposition might help to determine the cause.

One can image ferritin on graphene with LEEM and eV-TEM. The current resolution of eV-TEM is good enough to see ferritin molecules on graphene. If not, improving the resolution should make it possible to see ferritin molecules on graphene. One might need to clean the ferritin solution first just like that is necessary for the gold nanoparticles solution. Dialysis is an option for cleaning the ferritin solution.

If one is able to image ferritin, one can measure if one damages ferritin with low energy electrons and which combinations of electron energy and exposure time damage ferritin. One can also measure how the damage develops over time.

After being able to successfully image ferritin on graphene, one can look at other samples that are interesting to perform measurements on with low energy electrons like DNA, carbon nanotubes, polymer resist and other proteins.

Version of 18-08-2016– Created August 18, 2016 - 11:48

References

[1] Daniël Geelen, Aniket Thete, Oliver Schaff, Alexander Kaiser, Sense Jan van der Molen, and Rudolf Tromp. eV-TEM: Transmission electron microscopy in a low energy cathode lens instrument. *Ultramicroscopy*, 159:482–487, dec 2015.

[2] R.M. Tromp, J.B. Hannon, W. Wan, A. Berghaus, and O. Schaff. A new aberration-corrected, energy-filtered LEEM/PEEM instrument II. Operation and results. *Ultramicroscopy*, 127:25–39, apr 2013.

[3] Johannes Jobst, Jaap Kautz, Daniël Geelen, Rudolf M. Tromp, and Sense Jan van der Molen. Nanoscale measurements of unoccupied band dispersion in few-layer graphene. *Nature Communications*, 6:8926, nov 2015.

[4] Radosav S. Pantelic, Ji Won Suk, Carl W. Magnuson, Jannik C. Meyer, Philipp Wachsmuth, Ute Kaiser, Rodney S. Ruoff, and Henning Stahlberg. Graphene: Substrate preparation and introduction. *Journal of Structural Biology*, 174(1):234–238, apr 2011.

[5] Gerardo Algara-Siller, Ossi Lehtinen, Andrey Turchanin, and Ute Kaiser. Dry-cleaning of graphene. *Applied Physics Letters*, 104(15), 2014.

[6] R.M. Tromp, J.B. Hannon, A.W. Ellis, W Wan, A Berghaus, and O Schaff. A new aberration-corrected, energy-filtered LEEM/PEEM instrument. I. Principles and design. *Ultramicroscopy*, 110(7):852–861, jun 2010.

[7] Robert D Deegan, Olgica Bakajin, Todd F Dupont, Greb Huber, Sidney R Nagel, and Thomas a Witten. Capillary flow as the cause of ring stains from dried liquid drops. *Nature*, 389(6653):827–829, oct 1997.

[8] Alexandros Askounis, Khellil Sefiane, Vasileios Koutsos, and Martin E R Shanahan. Effect of particle geometry on triple line motion of nano-fluid

drops and deposit nano-structuring. *Advances in Colloid and Interface Science*, 222:44–57, 2015.

[9] N. Manivannan, W. Balachandran, C. Ribton, R. Beleca, M. Abbod, M. Cox, and P. Anastasia. Chromium coated silicon nitride electron beam exit window. *Vacuum*, 113:19–23, mar 2015.

Appendix A

Sample preparation details

In this appendix we give some extra information about the silicon nitride grids and the conductive coating.

Silicon nitride has a high melting point (2173 K), which means it is possible to heat the graphene on a silicon nitride grid in the microscope before measuring with LEEM or eV-TEM. This is only interesting with just graphene. Gold nanoparticles have a much lower melting point than bulk gold and melt and group together when heated. Ferritin denatures at a temperature well below that usually used to clean graphene.

Silicon nitride has a low thermal expansion coefficient of $3.3 \times 10^{-6}\,\mathrm{K}^{-1}$ [9] so we select metals with low thermal expansion coefficients close to that of silicon nitride. The thermal expansion coefficients of chromium, tungsten and titanium are $4.9 \times 10^{-6}\,\mathrm{K}^{-1*}$, $4.5 \times 10^{-6}\,\mathrm{K}^{-1*}$ and $8.6 \times 10^{-6}\,\mathrm{K}^{-1*}$ respectively.

In applying the conductive coating we use the Z-400 sputtering system as follows: we place the silicon nitride grids in the sputtering machine, pump it down until the pressure is roughly 5×10^{-6} mbar, let $\approx 5.3 \times 10^{-3}$ mbar argon in the vacuum and start sputtering. After sputtering we vent the machine, turn the grids upside down and repeat the process.

*David R. Lide (ed), *CRC Handbook of Chemistry and Physics*, 88th Edition, CRC Press, 2007

Appendix B

Alignment procedure

In this appendix we append a document we made for the aligning of the imaging system of ESCHER, for measuring the spherical and chromatic aberrations and for finding the correct parameters for the automatic adjustments of the electron mirror.

This document is based on Tromp et al. (2013) [2]. We copied the relevant parts of this article, changed the order of the text and added and removed explanations/details in order to make it a manual for aligning the imaging system and calibrating the aberration correction system. We did this for our own use during this project and we believe others that will do projects involving LEEM or eV-TEM can use this manual as well.

However we note that it is better to align the imaging system in the order described in subsubsection 2.3, which is the reverse of the order in this document. If you start at the sample and work your way to the detector, you start with correcting mistakes further on in the electron beam path and when you go closer to the detector and improve the alignment there you negate the 'improvements' you made earlier on.

We also note that this document assumes the starting position is a microscope that is not aligned at all. This means some things on the first two pages are irrelevant for optimising the alignment and in practice the general idea described in subsubsection 2.3 applies. This document contains more detailed instructions.

LEEM and eV-TEM aligning procedure and aberration correction

Made using *Tromp et al. - 2013 - A new aberration-corrected, energy-filtered LEEMPEEM instrument II. Operation and results*

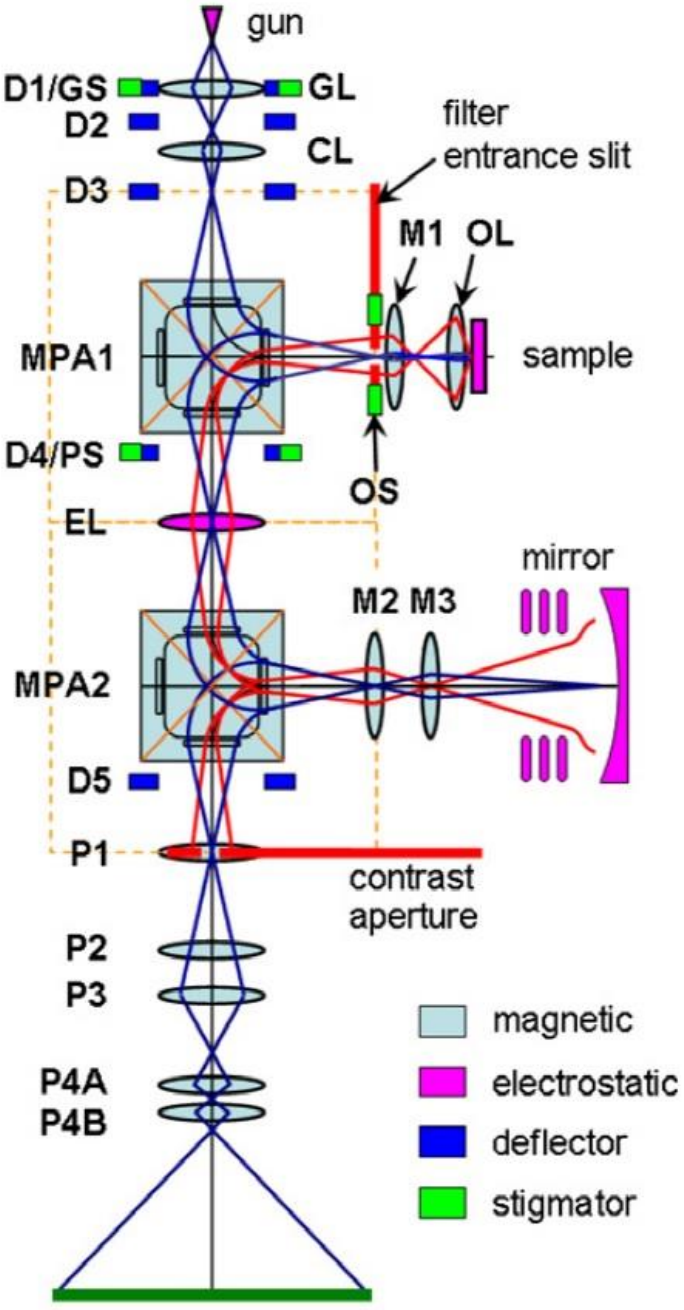

Fig. 1: Schematic view of the instrument

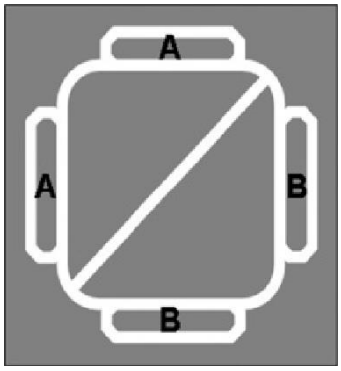

Fig. 2: MPA with four outer sectors and diagonally split inner sector. Each sector has its own excitation coil, but sectors 'A' are connected in series, as are sectors 'B'.

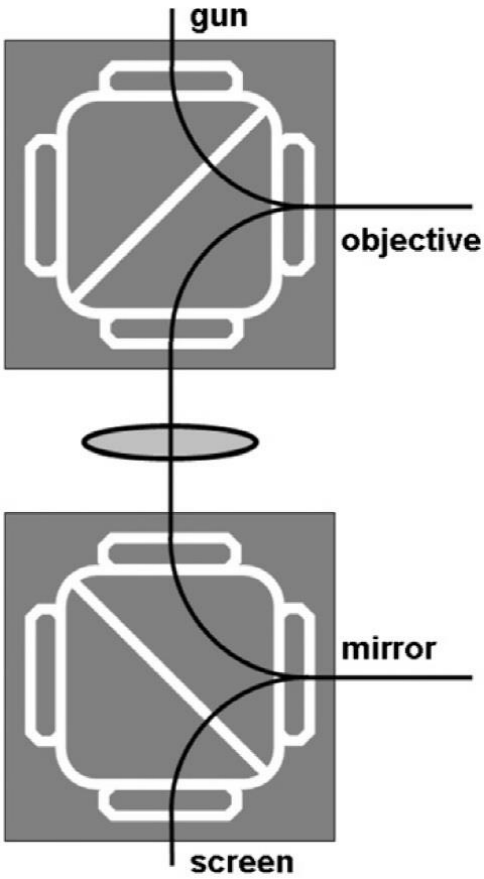

Fig. 3: The MPA's and the electron path in the LEEM.

Aligning the path of the electron beam from the gun (LEEM) or sample (eV-TEM) to the image screen, correctly stigmating the various optical components, and making sure that the image and diffraction planes are all in their correct positions.

3.1. Aligning MPA1 (assuming no alignment done yet)

Use PEEM to align the lower half of MPA1 (right-hand triangular sector and sectors 'B'— see Fig. 2)

- Settings: sample at -15 kV, OL (Objective Lens) and TL (Transfer Lens, M1 in fig. 1) at roughly the right excitation, MPA2 turned off and the projector lenses at roughly reasonable settings.
- Slowly increase the inner and outer MPA1 sector excitations in a ratio of 3.7 (in Ampereturns), with all apertures and grids retracted, until electrons make it through to the image screen and roughly focus the image.
- Switch to the diffraction plane and adjust the deflection angle of MPA1 to get the electron crossover centered on the viewing screen. Vary the inner+outer excitation while keeping the inner/outer ratio constant to adjust the deflection angle.
- Turn back to the image plane, insert the TEM grid in MPA1, focus on the grid with P2, and then focus the image more accurately with the objective lens.
- Remove the grid and go back to diffraction. By wobbling the excitation of P2 go back and forth in focus, viewing the electron crossover in the diffraction plane. If MPA1 is not stigmated, the crossover will display astigmatism as you go through focus. Adjust the ratio of outer/inner excitation of MPA1 (keeping the total deflection angle fixed) to stigmate the crossover until MPA1 is stigmated correctly.

Turn on the electron gun and switch to LEEM to align the upper half of MPA1 (left-hand triangular sector and sectors 'A'— see Fig. 2)

- Use D1 and D3 to steer the beam through the condenser optics, and adjust the upper half of MPA1 to put the beam on the sample. Usually, it is sufficient to slightly adjust the excitation of the upper left-hand triangular sector and sweep the electron beam across the sample. It may also be helpful to defocus the gun lens so that a broad area of illumination is obtained.
- Once the beam is found, use D1 and D3 to control the angle of incidence and center of illumination.
- Vary the outer/inner excitation in the upper half of MPA1 (i.e. stigmating that part of MPA1) to adjust the beam shape. (As the lower half of MPA1 has already been aligned and stigmated, leave those settings unchanged as you adjust the electron beam.)

3.2. Aligning MPA2 using PEEM (gun turned off or blanked)

- Settings (roughly correct): ETL (EL (Electrostatic transfer Lens) in fig. 1) = -8820 V, MTL1 (M2 in fig. 1) = MTL2 (M3 in fig. 1) = 700 Ampereturns, V1 = -1600 V, V3-V2 = 3000 V and V2 = 1400 V (voltages are relative to the column potential of -15000 V). (When applying high voltages to the ETL and to the electron mirror components *for the first time*, it is important to slowly and carefully condition these elements. Turn the voltages up in small increments, and wait if any discharges occur, until they stop. Discharges can usually be discerned by keeping an eye on the vacuum pressures in the relevant parts of the system. If discharges can be heard, back off instantly. It can take 2 days to reach full voltage. In day to day operation, turning up the mirror takes a few minutes.)
- Set the outer elements of MPA2 at one excitation and the two inner triangles at a ratio of 3.7 with respect to the outer elements.
- Wait until MPA2 has ramped up and electrons reach the screen after two 90° deflections.

- Apply a voltage wobble to the final mirror electrode to go back and forth through focus. Insert the TEM grid in the MTL2 plane to observe the shadow of the TEM grid cast by the electrons on their way to the mirror. (You also see the return shadow, but this is not affected by the mirror.) Going through focus there is strong astigmatism in the grid image and a noticeable image shift.
- Tie together all outer sectors and also the two inner triangles, adjust the outer/inner excitation of MPA2 to remove astigmatism, and the inner+outer excitation to minimize image shift. (The astigmatism is a combination of MPA2 astigmatism and off-axis incidence on the mirror. Varying the outer/inner ratio stigmates MPA2, while the inner+outer excitation varies the deflection around a 90° angle.)
- MPA2 is adjusted to improve the situation as much as possible. However, in general there will still be a slight image shift remaining, predominantly in one direction (orthogonal to the deflection direction of the prism array).
- Adjust D4 to remove this remaining image shift.
- Adjustment of MPA2/D4 can be iterated a few times to obtain optimum results.
- When done, things should look like a stigmatically breathing, stationary image of the MTL2 grid.

3.3. Focusing the electron mirror using PEEM (gun turned off or blanked)

- Insert the TEM grid on the upper diagonal of MPA2 (with the TEM grid in the MTL2 plane still inserted).
- Both incident and return MTL2 grid image and the TEM grid on the upper diagonal of MPA2 should be in focus. If not, adjust MTL1.
- Insert the TEM grid on the diagonal of MPA1 and focus with ETL.
- Focus the sample image with the objective lens and stigmate with the objective lens stigmator.
- Switch the projector column to diffraction. The beam crossover should be visible as before. It should also be close to being stigmated. Fine-tune this by adjusting the bottom half (right-hand triangular sector and sectors ‘B’) of MPA2.
- Since the electrons do not pass through the bottom half of MPA2 on their way to the mirror, this does not affect the alignment already done. If needed, fine-focus the diffraction plane by adjusting MTL2.
- If there is a slight astigmatism out of the deflection plane of MPA2, adjust PS. Experience shows this astigmatism is very minor if at all distinguishable and is easily corrected.
- Check again if the electrons are incident on the mirror on-axis and fine-tune D4 one more time.
- Turn on the electron beam again and it will hit the sample as before, since we did not make any changes in the gun-sample-MPA1 alignment.
- Center the beam with a small adjustment in D1 and D3 and set the desired angle of incidence. If the sample has a clean, crystalline surface, the LEED pattern can be observed in the diffraction plane.

3.4. Double checking the setup using PEEM (gun turned off or blanked)

1. Insert an energy filter slit in the entrance plane of MPA1. Place the slit so that the largest possible field of view is visible in the image. The assumption is that the diffraction plane is located in the filter slit plane. To make sure that it is, vary the excitation of TL. If TL is underfocused, the diffraction plane will be focused between the filter entrance slit and MPA1, and the filter slit will cut off the edges of the image. The same situation arises when TL is overfocused and the diffraction plane is in focus to the right of the slit. Taking TL through focus, you will see the image being cut off in underfocus, expanding as we approach focus, filling the screen in focus, and getting cut off again in overfocus. Focus TL by maximizing the field of view

transmitted by the filter slit. After focusing TL you may have to slightly adjust the objective lens focus to maintain image focus.

2. Insert the TEM grid on the lower diagonal of MPA1. The grid and the sample image must both be in focus. Additionally, if you use a sample with a calibrated magnification standard (such as a silicon wafer with lithographically defined artwork), you can measure the magnification on the prism diagonal directly. You can proceed in two ways: you can displace the grid over a known distance, using the calibrated micrometer drives used to operate the aperture drive, to measure this distance on the prism diagonal, and compare that with the known size of a feature on the sample. Or you can use the known TEM grid periodicity and compare it to the known feature size on the sample. Either way, you obtain a direct measurement of the magnification of the real image on the prism diagonal. This magnification must be 26.9 (i.e. $38/\sqrt{2}$). If the magnification is too large (too small), it indicates that the sample is too close to (too far from) the objective lens, and the objective-sample spacing must be adjusted until the correct magnification is obtained.
3. Insert the TEM grid on the upper diagonal of MPA2. This must now also be in focus, and must appear with the same magnification as the MPA1 grid. If that is not the case, adjust the excitation of EL.
4. Remove the MPA1 grid and insert the MTL2 grid. It too must be in focus (both before and after reflection by the electron mirror). The magnification in the MTL2 plane must be 8.5 for the correction optics to work as designed. If the magnification on the prism diagonal is correct, then the magnification in the MTL2 plane is automatically correct. Nonetheless, you can check that this is so by comparing the magnification of the TEM grid on the MPA2 diagonal with that of the MTL2 TEM grid. The ratio must be $36/\sqrt{2}/8.5 = 3.16$. Experimentally, Ruud Tromp measured a ratio of 3.14, within 1% of theory. Notice that you can check this magnification ratio without reference to the sample, just by looking at the shadows of the TEM grids. Since both TEM grids are located in image planes, they are in focus at the same time and measuring the magnification ratio is trivial.
5. Take all the grids out and look at the sample image. Now wobble the excitation of ETL. The electrons must pass through the center of that lens. If they do not, the image will shift back and forth as the lens is wobbled. If necessary, adjust MPA1 and MPA2 together (keeping all relative excitations fixed) until the image stops shifting. Now the electrons pass through the center of ETL.
6. With the TEM grid in MTL2 inserted, wobble mirror voltage V1. The grid images must stand still and breathe stigmatically. If not, adjust D4.
7. Finally, you want to make sure that MTL2 is focused correctly. You can assess this by inserting a contrast aperture at the center of P1. The procedure is very similar to focusing TL. When MTL2 is properly focused, it will return the diffraction plane to the center of MTL1, and MPA2 will place it in the plane of the contrast aperture. But when MTL2 is underfocused (overfocused), the diffraction plane will be in focus below (above) the contrast aperture plane, and the contrast aperture will cut off the outer edges of the image. So you can take MTL2 through focus and find the proper excitation at which the field of view transmitted through the contrast aperture is maximized. This focuses MTL2. Proper focus of MTL1 is assured by the condition that the images of the TEM grids in MPA2 and MTL2 are in focus at the same time.

Correcting chromatic and spherical aberrations

4.1 Mirror optics

The above procedure was done for a particular setting of the voltages applied to the mirror electrodes. However, in general these values of C_c and C_3 will not match the aberrations of the objective lens. The spherical aberration coefficient of the mirror depends to first order on the voltage difference V3 – V2 (in the following, V32 = V3 – V2), while the chromatic aberration coefficient depends to first order on V1. V2 focuses the mirror. Thus, you are able to vary C_c^m and C_3^m independently. Additionally it should be noted that the objective lens aberration coefficients relative to the image at the center of MTL2 depend strongly on magnification M: *C_3 increases with M^4, and C_c with M^2*. For this reason it is essential that the image magnification *in the MTL2 plane is accurately controlled.*

If you establish the relationship between electron energy and mirror excitation, then the mirror voltages can track electron energy in software. To make adjusting C_c^m and C_3^m easier, an algorithm can be implemented that controls the voltages applied to the mirror electrodes by specifying the desired values of C_c^m and C_3^m.
You can thus construct a data set specifying V32(C_c^m, C_3^m) and V1(C_c^m, C_3^m). These data sets can then be fitted with 5th order polynomials. These polynomials can be coded into the computer control software to set V32 and V1 for a desired setting of C_c^m and C_3^m .
In practice, C_c^m and C_3^m are controlled through software sliders that adjust the mirror voltages using the polynomial fits. The only free variable is then the absolute value of V2 which controls the focal length. However, V2 is also a unique function of (V32, V1) and this too can be fitted with a fifth order polynomial. As a result, C_c^m and C_3^m can be controlled directly through the user interface, while at the same time keeping the mirror in focus.

This procedure also allows the user to quickly assess the result of aberration correction, as the mirror aberration coefficients can easily be set to zero (uncorrected operation). No changes in microscope alignment or electron beam path are required to do this, as all you have to do is to set the voltages required to set C_c^m and C_3^m to zero.

4.2.1 Systematic correction of spherical aberration

To correct the aberrations in a systematic manner, we must have some way of measuring and inspecting them directly. When a ray leaves the sample on the optical axis at an angle α, if does not intersect the optical axis in the Gaussian image plane, but it suffers a small displacement δ. This displacement is given by $\delta = C_1\alpha + C_3\alpha^3 + \cdots$, where C_1 is the objective lens defocus.

This displacement δ can be measured as a function of α by tilting the illuminating beam on the sample over a range of tilt angles. While this method works in principle, it is very cumbersome in practice, and it is not so easy to obtain good results. Rather than illuminating the sample with a broad beam, insert a 5 µm aperture in the upper diagonal of the top prism, which results in a small illumination spot of 0.2 µm diameter on the sample. Select a sample with a rich diffraction pattern, e.g. Si(111)-(7x7) which can be easily and quickly prepared in the LEEM system, and is stable over extended periods of time. The fractional order diffracted beams, with accurately known angles relative to the (0,0) beam, each contribute to the image of the illuminated spot formed by the cathode lens. As a diffracted beam is further away from the optical axis, it will form an image which is radially displaced further from the (0,0) image as a result of spherical aberration. That is, each diffracted beam is reflected in the image plane by an image that is shifted from the on-axis (0,0) image, with the shift determined by spherical aberration. Of course, the shift also contains a term due to objective lens defocus. Fig. 4 shows several examples of

such images, with an over-focused objective lens. The electron energy in these images was 5.4 eV. The inset at the center of Fig. 4 shows the LEED pattern which was identical for images (a)–(d). We stress that images (a)–(d) look like distorted LEED patterns, but they are not. They are over-focused images of the collimated, small diameter electron beam illuminating the sample.

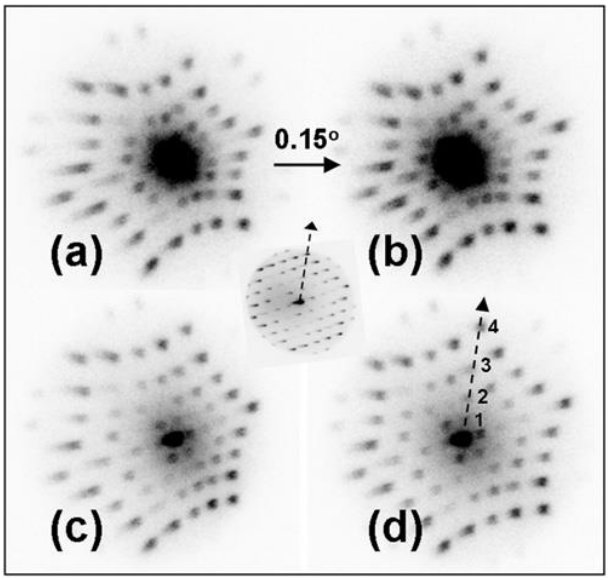

Fig. 4. (a–d) Over-focused images of a 200 nm diameter beam illuminating a Si(111)(7x7) sample at an electron energy of 5.4 eV. (a) and (b) C_3^m set to zero. The asymmetry in (a) is due to sample tilt. This is corrected in (b) by a tilt of 0.15°. The asymmetry in (c) is due to off-axis incidence on the mirror, with C_3^m set to -1000. This is corrected in (d). The center inset shows the LEED pattern.

The non-linearity of these images directly reflects spherical aberration. Images (a) and (b) were obtained with C_3^m set to zero. (Experimentally, we can see that this is indeed so by changing the excitation of D4, i.e. the angle of incidence on the mirror. Fig. 4a does not change upon changing D4, showing that indeed C_3^m = 0.) Thus, the mirror does not contribute to the distortion of the image. The lack of symmetry in (a) is entirely due to sample tilt. If the sample is slightly tilted relative to the optical axis, the (0,0) diffracted beam, leaving along the surface normal, will not coincide with the optical axis even though it is centered in the Ewald sphere. All the other diffracted beams will be shifted relative to the optical axis as well, with some beams closer to the axis than they should be, and other beams further away. This gives rise to the lack of symmetry seen in (a). A small correction in sample tilt by 0.15° between (a) and (b) removed this misalignment.

Next we changed C_3^m from 0 to -1000 m, and observed image (c). Again, the image is not symmetric. This time, the asymmetry is not due to sample tilt, but due to misalignment of the (0,0) beam relative to the optical axis of the electron mirror. Adjustment of deflection coil D4 readily fixes this problem, resulting in Fig. 4d. We have now adjusted both the sample tilt and the incidence angle on the electron mirror to achieve a well-aligned setup. Since these images can be observed in real time, and contain information along all azimuthal directions, we can quickly assess and correct any misalignment.

Next, we can vary C_3^m . Fig. 5 shows images obtained for C_3^m settings of 0, -1000, and -2100 m, increasingly removing non-linearity from the image. The microscope is almost fully corrected in Fig. 5c.

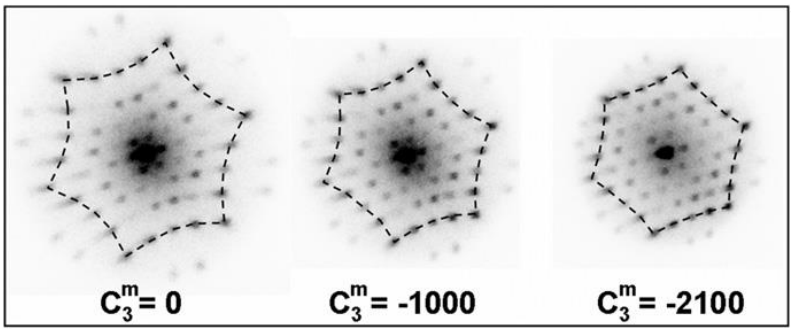

Fig. 5. Over-focused small-spot illumination images for different C_3^m settings of the electron mirror. The dashed lines highlight the decrease in distortion with increasingly corrected C_c.

A single image, taken at one defocus setting, contains sufficient information to extract defocus and spherical aberration at the same time, as shown in Fig. 6 for C_3^m = 0. One 60° wedge out of the image contains the images corresponding to 15 diffracted beams from (0,0) up to 4/7 order. The angles with the optical axis are accurately known for all 15 beams. We can extract the displacement for each of these beams relative to the (0,0) image, as shown in Fig. 6, and fit with $\delta = C_1\alpha + C_3\alpha^3$. The fit yields a defocus C_1 = 122.5 ± 10 µm, and C_3 = 0.39 ± 0.04 m, in very good agreement with results of more elaborate measurements.

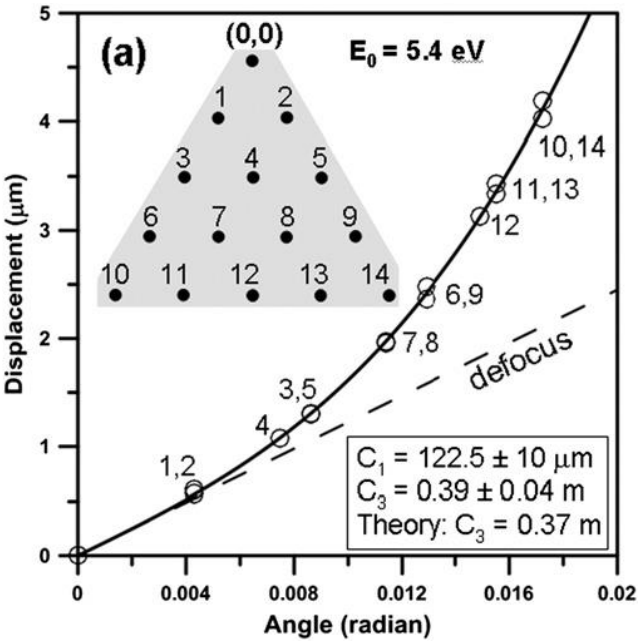

Fig. 6. Radial displacement of over-focused small spot image for 15 different diffracted beams. The fit to the data extracts both defocus C_1 (dashed line) and C_3 with good accuracy.

There is no need for a-priori knowledge of defocus, making the measurement insensitive to the exact defocus setting and easier to do in practice. Now we can take *single* defocused images as a function of the spherical aberration setting of the electron mirror to measure the degree of correction quickly and accurately.

Fig. 7a shows a measurement of the objective lens C_3 as a function of E_0, compared with theoretical values, and fitted with a function of the form $C_3 = a + b/\sqrt{E_0}$. The value of C_3^m that corrects the C_3 aberration of the objective lens is given by $C_3^m = -C_3 M^4$, where M is the magnification in the object plane of the mirror with a nominal value of 8.5. Fig. 7b shows the total value of C_3 as a function of C_3^m. We see a linear decrease in C_3 as C_3^m is increased. The slope of the fitted line, 0.0001472, equals $1/M^4$, yielding M = 9.07, slightly higher than the nominal value of 8.5. A small adjustment of the sample-objective lens spacing suffices to correct the magnification.

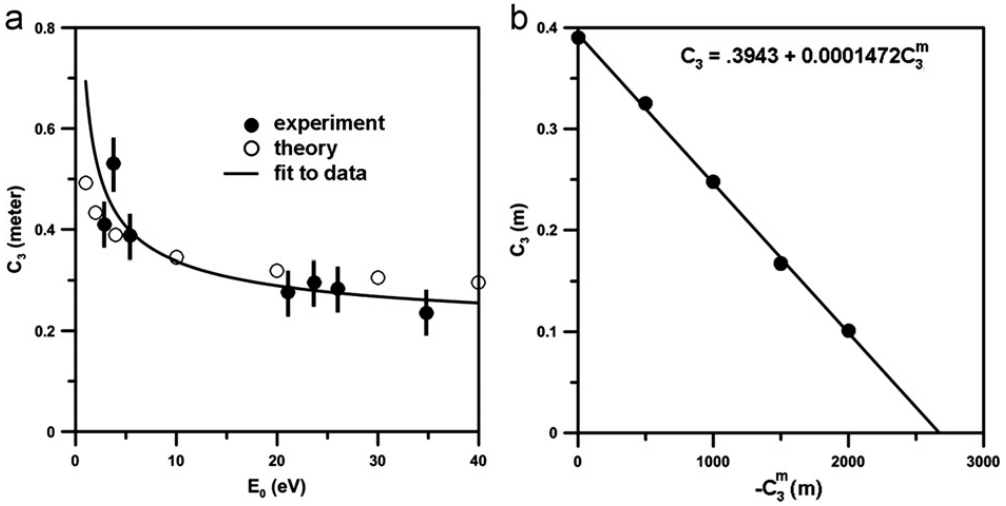

Fig. 7. (a) Measurements of objective lens C_3 (with C_3^m set to zero) as a function of start energy E_0 (solid symbols). Also shown are theoretical values of C_3 (open symbols) and a fit to the data (line). Experiment agrees well with theory. (b) Measured total value of C_3 at E_0 = 5.4 eV as a function of C_3^m.

4.2.2. Systematic correction of chromatic aberrations

Measuring and correcting C_c is somewhat more complicated. C_c consists of a start energy-dependent part due to the electrostatic field between objective lens and sample, and a start energy-independent part due to the magnetic part of the objective lens. The second part is easy to measure with Hg PEEM by recording the change in objective lens excitation required to keep the image in focus as the voltage applied to the sample is varied. In this case the start energy of the electrons is fixed, and we only see the sum of the magnetic lens aberration and the mirror aberration.

Fig. 8 shows the result of such measurements as we vary C_c^m. Using the aforementioned polynomials, we can set C_c^m, keeping C_3^m fixed at -2000 m. We set C_c^m at values from 0 to 10 m, and measured the changes in objective lens focus as a function of sample voltage for these different settings (Fig. 8a). As the electrostatic field between the sample and the objective lens is almost constant, this measurement is sensitive to the chromatic aberration coefficients of the magnetic part of the objective lens and the electron mirror. In Fig. 8b we plot the slopes of the lines in Fig. 8a as a function of C_c^m, showing a linear dependence as expected. The different symbols in Fig. 8b were measured for different settings of C_3^m. The results are independent of C_3^m, showing effective decoupling in the set values of C_c^m and C_3^m, The fit to the data is of the form $S = S_0 - aC_c^m$.

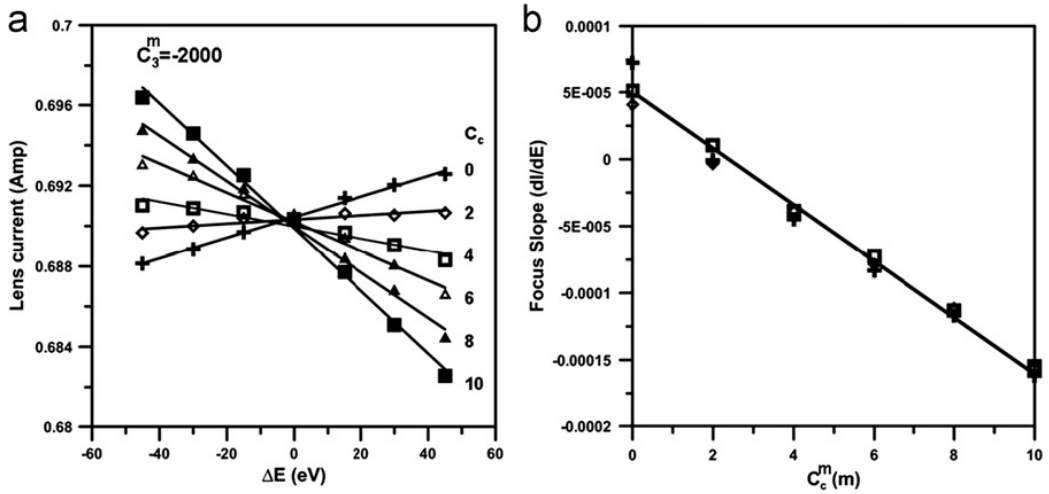

Fig. 8. (a) Change in objective lens current vs change in sample potential as a function of C_c^m , measured with Hg PEEM. ΔE = 0 corresponds to a sample potential of 15,000 V. As C_c^m is increased, the slope of the data changes sign. (b) Slope of the lines in (a) vs the setting of the chromatic aberration coefficient of the mirror. Different symbols are for different C_3^m settings: plusses C_3^m = 0 m, diamonds C_3^m = -1000 m, squares C_3^m = -2000 m. The fit to the slope is of the form $S = S_0 - aC_c^m$.

The chromatic and spherical aberrations of the objective lens depend both on the final energy of the electrons, after acceleration into the objective lens, and on the energy with which the electrons leave the sample. Fig. 9a shows the change in objective lens current in a LEEM experiment in which the start energy E_0 is varied, but the final column energy is held constant. These focusing curves are measured for different setting of C_c^m. As the electrons reach the mirror at a fixed electron energy (i.e. independent of E_0), the data are insensitive to the setting of the mirror. The solid line through the data is a fit of the form $I = I_0 + c\sqrt{E_0}$.

At a given value of E_0 the chromatic aberration coefficient of the objective lens is corrected when the *sum* of the slope of the data in Fig. 9a (i.e. $dI/dE = c/(2\sqrt{E_0})$ and the slope at E_0 plotted in Fig. 8b equals zero, i.e. $c/(2\sqrt{E_0}) + S_0 - aC_c^m = 0$. The value of C_c^m extracted from this last equation corrects the chromatic aberration of the objective lens at energy E_0.
When the microscope is corrected, the value of $-C_c^m$ equals the chromatic aberration coefficient of the objective lens times the magnification in the object plane of the mirror squared, i.e. $C_c = -C_c^m/M^2$.

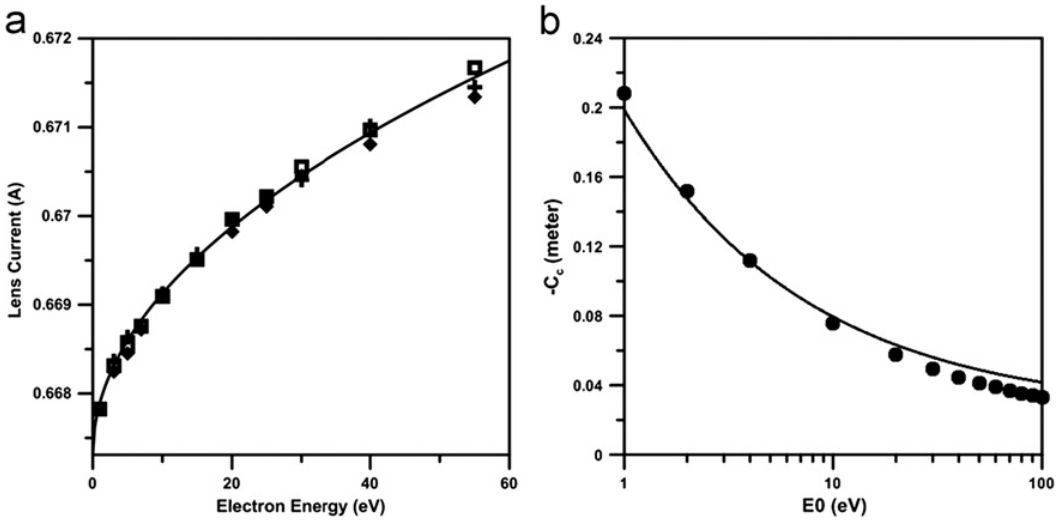

Fig. 9. (a) Objective lens current as a function of start energy E_0 in a LEEM experiment. Different symbols are for different settings of C_c^m; diamonds: 0 m, plusses: 5.8 m, squares: 10 m. The fit is of the form $I = I_0 + c\sqrt{E_0}$. (b) Chromatic aberration coefficient of the objective lens as a function of E_0. Solid line obtained from measurements as shown in Figs. 8 and 9a; solid circles are theoretical values obtained by raytracing.

Fig. 9b shows the result of such measurements. The solid line is $-C_c^m/M^2$ extracted from measurements as presented in Figs. 8 and 9a, with M = 8.5. The solid symbols are theoretical values of the chromatic aberration coefficient of the objective lens. Again, we find good agreement between theory and experiment. The agreement seen in Fig. 9b, obtained by directly linking C_c of the objective lens (through Fig. 9a) with C_c^m (through Fig. 8), with the magnification M as the only parameter (taken here at its nominal value of 8.5), vividly demonstrates that the electron mirror indeed operates in very close agreement with the theory. That is, an accurate experimental realization of the theoretical first order focusing properties of the electron mirror also guarantees an accurate reproduction of its chromatic and spherical aberration coefficients.
As Figs. 8b and 9a also demonstrate, the polynomial expression for V1 and V3 - V2 indeed gives us independent control of the chromatic and spherical aberration coefficients of the electron mirror, allowing full implementation of Automatic Tracking Aberration Correction (ATrAC), in which the voltage settings of the electron mirror are programmed to automatically track the changes in the aberration coefficients of the objective lens as E_0 is varied. This removes the arduous task of keeping the microscope corrected during routine instrument operation. As long as the magnification of the image in the object plane is carefully controlled, the microscope software can handle the rest.

4.2.3. Magnification calibration

In the above we have commented on the importance of controlling magnification as accurately as possible. The electron mirror corrects the aberrations of the image located in the mirror object plane, with magnification M (nominally M = 8.5). Since C_c (C_3) scales with M^2 (M^4), tight control over M is required. Here we make a few brief remarks on how we measure and calibrate magnification. First, using lithographically patterned Si wafers, it is straightforward to calibrate magnification in the range down to several micrometers. To measure magnification in the principal planes (diagonal of MPA1, object plane of the mirror at the center of MTL2), we compare features of known size on the sample with the spacings of TEM grids inserted in those planes. Particularly useful are the Pelco Holey silicon nitride support films for TEM available from Ted Pella, Inc. These support films have extended fields consisting of 2.5 µm diameter holes at 4.5 µm spacings in a hexagonal grid. We have used these support

films as evaporation masks to produce patterned Ti/Au grids on silicon substrates that can be observed with either PEEM or LEEM. After Ti/Au coating, these grids can also be used as a reference on the diagonal of MPA1.
This has the great advantage that a common standard is used for the sample, and for the key reference planes. The magnification can be measured directly as shown in Fig. 10. Once the magnification from sample to MPA1 has been measured and set to 26.9 (in the *real* image plane), the nitride window on the diagonal of MPA1 can be used to calibrate magnifications to fields of view well below 1 µm. Additionally, the sample stage has x–y position encoders with a read-out accuracy of a few nanometers. Thus, at any magnification we can make a known excursion with the x-y stage and measure the corresponding shift of the image, giving another direct measurement of the magnification.

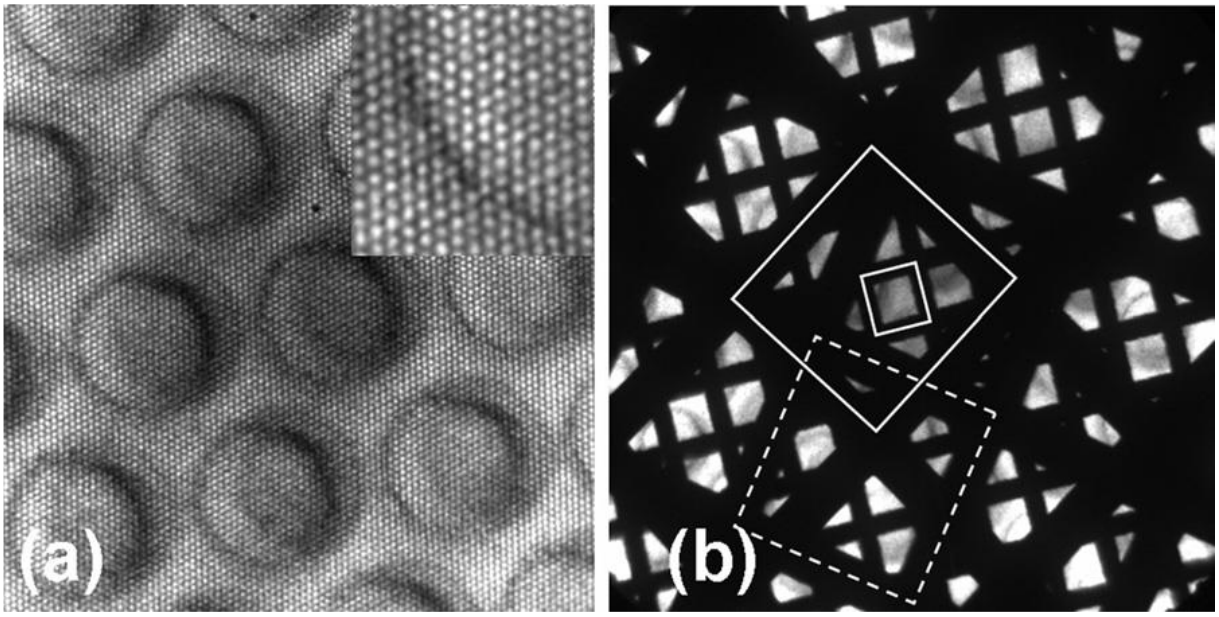

Fig. 10. (a) PEEM image of a sample (fabricated by shadow mask evaporation through a Pelco grid with large circles at 4.5 mm spacings) after passing through the same Pelco grid inserted on the diagonal of MPA1. The inset shows a magnified portion of the image. The magnification from sample to diagonal can be directly measured from this image: M = 26.5 ± 0.5, close to the design value of 26.9. (b) Simultaneous shadow images of identical TEM grids placed on the diagonal of MPA1 (small squares) and the object plane of the mirror (two rotated sets of large squares). The demagnification from the MPA diagonal to the mirror object plane can be measured directly from this image. The sample image is seen in the background.

To measure the demagnification between the prism diagonal and the object plane of the mirror, we insert identical TEM grids in both locations. An example of the resulting image is shown in Fig. 10b. In total we see three grid shadow images. The first is the fine image of the grid on the MPA1 or MPA2 diagonal (small solid white square). The second, coarser grid image is formed by the electrons as they approach the mirror (dashed white square), and the third as they return from the mirror (large solid white square). With the mirror and the transfer optics properly focused, these three images are in focus at the same time. The demagnification from MPA diagonal to mirror is measured directly from the relative dimensions of the grid squares in (b). In the background we see the focused image of the same sample as in (a).